

# Paleoceanography and Paleoclimatology\*



## RESEARCH ARTICLE

10.1029/2025PA005125

### Key Points:

- The accuracy of existing proxy-based dissolved inorganic carbon (DIC) reconstruction methods depends strongly on the scale and process of environmental perturbation
- Without a second carbonate system parameter, carbonate ions are a poor proxy of DIC change on centennial to glacial-interglacial timescales
- DIC change is not a general indicator of atmospheric CO<sub>2</sub> drawdown

### Supporting Information:

Supporting Information may be found in the online version of this article.

### Correspondence to:

M. Adloff,  
[markus.adloff@bristol.ac.uk](mailto:markus.adloff@bristol.ac.uk)

### Citation:

Adloff, M., Jeltsch-Thömmes, A., Rae, J. W. B., Pöppelmeier, F., Trudgill, M., Stocker, T. F., & Joos, F. (2025). Evaluating glacial CO<sub>2</sub> system reconstructions from benthic proxies in earth system simulations. *Paleoceanography and Paleoclimatology*, 40, e2025PA005125. <https://doi.org/10.1029/2025PA005125>

Received 29 JAN 2025

Accepted 8 SEP 2025

### Author Contributions:

**Conceptualization:** M. Adloff, A. Jeltsch-Thömmes, F. Joos

**Data curation:** M. Adloff

**Formal analysis:** M. Adloff

**Funding acquisition:** F. Joos

**Investigation:** M. Adloff, A. Jeltsch-Thömmes, J. W. B. Rae, F. Pöppelmeier, T. F. Stocker, F. Joos

**Methodology:** M. Adloff, A. Jeltsch-Thömmes

**Project administration:** F. Joos

**Software:** M. Adloff

**Supervision:** F. Joos








**Visualization:** M. Adloff

**Writing – original draft:** M. Adloff, F. Joos

© 2025. The Author(s).

This is an open access article under the terms of the [Creative Commons Attribution License](#), which permits use, distribution and reproduction in any medium, provided the original work is properly cited.

## Evaluating Glacial CO<sub>2</sub> System Reconstructions From Benthic Proxies in Earth System Simulations

M. Adloff<sup>1,2,3</sup> , A. Jeltsch-Thömmes<sup>1,2</sup> , J. W. B. Rae<sup>4</sup> , F. Pöppelmeier<sup>1,2</sup> , M. Trudgill<sup>5</sup> , T. F. Stocker<sup>1,2</sup> , and F. Joos<sup>1,2</sup> 

<sup>1</sup>Climate and Environmental Physics, Physics Institute, University of Bern, Bern, Switzerland, <sup>2</sup>Oeschger Centre for Climate Change Research, University of Bern, Bern, Switzerland, <sup>3</sup>Now at: School of Earth Sciences, University of Bristol, Bristol, UK, <sup>4</sup>School of Earth and Environmental Sciences, University of St. Andrews, St. Andrews, UK, <sup>5</sup>Laboratoire des Sciences du Climat et de l'Environnement (LSCE/IPSL), Paris, France

**Abstract** Reconstructing marine dissolved inorganic carbon (DIC) across glacial cycles is critical for understanding the sensitivity of the marine carbon sink to natural climatic change. Published estimates of DIC invoke linear relationships between DIC and CO<sub>3</sub><sup>2−</sup>, apparent oxygen utilization (AOU), or δ<sup>13</sup>C. These relationships are based on conceptual models and correlations from modern spatial tracer gradients. However, it remains unclear whether the spatial correlations also hold for temporal change. Here, we apply these empirical methods to Earth system model results to test their applicability to transient glacial-interglacial changes. The model uses established, experimentally-constrained carbonate system solvers and explicitly tracks the various components of the carbon cycle (e.g., DIC, alkalinity, temperature, CO<sub>2</sub>). Predicting simulated DIC from simulated CO<sub>3</sub><sup>2−</sup>, AOU, or δ<sup>13</sup>C often results in large prediction errors. The interplay of the carbonate system, ocean circulation, and biologically-mediated DIC and alkalinity re-distributions creates a system too complex to be captured by existing empirical methods. Specifically, large local alkalinity changes can arise due to circulation and export production changes even without substantial changes in global mean alkalinity. Consequently, reconstructed CO<sub>3</sub><sup>2−</sup> constrains DIC changes insufficiently. Similarly, marine AOU or δ<sup>13</sup>C are not reliable proxies of remineralized DIC. Furthermore, DIC changes are not a direct metric for atmospheric CO<sub>2</sub> drawdown even without considering changes in global mean alkalinity because of net carbon exchange with sediments and the land biosphere. We suggest that spatially-resolved, transient Earth system simulations may provide a more reliable means of estimating carbon cycle shifts observed in proxy data than current empirical methods.

**Plain Language Summary** Atmospheric CO<sub>2</sub> varied substantially over glacial-interglacial cycles as shown by ice core data. The exact causes of these past CO<sub>2</sub> variations remain unknown but are shown to be related to large-scale reorganizations of the ocean carbon cycle. A difficulty is that past ocean carbon cannot be directly measured but is estimated from proxy data. We tested three published methods of calculating how much carbon was dissolved in the ocean during ice age cycles. For this, a model of the Earth system is applied to represent plausible real-world processes of the ocean carbon cycle and ocean-sediment interactions. The results show that none of the methods is generally correct because the way that carbon and proxy signals in the ocean change over time is more complex than the carbon-proxy correlations inferred from modern ocean observations. We discuss the processes that create this complexity and suggest the best way forward is to estimate carbon changes in the ocean from proxy data by using spatially resolved Earth system models rather than simple correlations.

## 1. Introduction

Quantifying the carbon transfer from the atmosphere to other carbon reservoirs during glacial periods remains an ongoing challenge. A robust understanding of how these reservoirs changed is essential for identifying the processes that sequestered carbon during glacial intervals and released it back to the atmosphere during deglaciations. As the largest carbon reservoir at Earth's surface that exchanges carbon directly with the atmosphere, the ocean has long been recognised as a key player in glacial atmospheric CO<sub>2</sub> changes (Knox & McElroy, 1984; Sarmiento & Toggweiler, 1984; Siegenthaler & Wenk, 1984). However, the specific processes governing oceanic carbon storage during glacials remain largely under-constrained.

**Writing – review & editing:** M. Adloff, A. Jeltsch-Thömmes, J. W. B. Rae, F. Pöppelmeier, M. Trudgill, T. F. Stocker, F. Joos

Extensive efforts have provided crucial proxy constraints on glacial marine carbon cycling. Yet, there is no direct indicator for Dissolved Inorganic Carbon (DIC), and it therefore has to be inferred more indirectly. There is now quantitative data on carbon isotope ( $\delta^{13}\text{C}$ , e.g., Emerson and Archer (1992), Schmittner et al. (2017), Peterson and Lisiecki (2018) and  $\Delta^{14}\text{C}$ , e.g., Skinner et al. (2017), Rafter et al. (2022)), benthic carbonate ion ( $\text{CO}_3^{2-}$ , e.g., Yu and Elderfield (2007)), oxygen ( $\text{O}_2$ ) and phosphate ( $\text{PO}_4^{3-}$ ) concentrations (Bradtmeier et al., 2010; Jaccard et al., 2009; Vollmer et al., 2022) and pH changes (Anagnostou et al., 2012; Hönisch et al., 2012; J. W. Rae et al., 2018; Shao et al., 2019; Yu & Elderfield, 2007, and references therein), all with steadily increasing spatial and temporal coverage. The growing availability of such reconstructions is crucial for understanding how marine carbon storage responded to the dramatic environmental changes of past ice age cycles.

Recent efforts have focused on interpreting the reconstructed proxy signals quantitatively, estimating absolute changes in DIC and ocean carbon storage. These estimates are typically derived using calibrations based on laboratory experiments, spatial gradients in the present-day ocean, or established process-based conceptual models. The latter approach includes analysis of preformed and regenerated tracers, which are linked by stoichiometric ratios. For instance, DIC produced by remineralization of organic matter has been quantified from Apparent Oxygen Utilization (AOU, Anderson et al., 2019; Gottschalk et al., 2020; Ito & Follows, 2005; Vollmer et al., 2022) or inferred from modern relationships between  $\Delta^{14}\text{C}$  water mass age and carbon storage (Sarnthein et al., 2013; Skinner et al., 2017).  $\text{CO}_3^{2-}$  changes are often converted to DIC changes by applying the spatial relationship observed between the difference in alkalinity (ALK) and DIC (ALK minus DIC), and  $\text{CO}_3^{2-}$  concentrations in the modern Atlantic (Yu et al., 2016), while assuming constant ALK globally and locally (Farmer et al., 2019; Lacerra et al., 2017; Yu et al., 2016, 2023). Assumptions are necessary to solve the carbonate system due to incomplete constraints, but the uncertainties introduced by these assumptions are often unclear and have not been rigorously assessed.

An important challenge lies in the limited observational data available to test whether tracer relationships based on present-day spatial gradients,  $dT/dx$ , can reliably be applied to reconstruct past temporal changes,  $dT/dt$ , and how much and fast unconstrained carbonate system parameters like ALK change through time. The following questions arise: Are these inferred relationships valid for reconstructing tracer evolution under different physical and biogeochemical boundary conditions? How do factors such as ocean circulation, exchange with ocean sediments, and burial-weathering imbalances affect these relationships? Similarly, how much does local ALK vary over time, and what is the magnitude of error introduced in DIC reconstructions by assuming constant ALK?

The strongest and simplest assumption is of a closed atmosphere-ocean (neglecting marine sediments, lithosphere, and the land biosphere) system to reconstruct past DIC changes, such that reconstructed DIC variations directly translate to atmospheric  $\text{CO}_2$  changes. Under this assumption, a one-to-one relationship between the moles of carbon stored DIC and the net carbon flux into the ocean through the air-sea interface can be used to equate DIC changes with atmospheric  $\text{CO}_2$  loss or gain (e.g., Ito & Follows, 2005; Vollmer et al., 2022). However, when carbon fluxes across the sea-sediment interface are additionally considered, no a-priori one-to-one relationship exists between the magnitude and timing of marine carbon storage changes and air-sea gas exchange. In particular, variations in sedimentary carbon storage, both as  $\text{CaCO}_3$  and organic C, can substantially alter DIC independently of atmospheric  $\text{CO}_2$ , potentially resulting in DIC changes that far exceed carbon storage changes observed in the atmosphere and terrestrial biosphere combined (Adloff, Jeltsch-Thömmes, et al., 2024a, 2024b).

Model sensitivity studies can help advance the understanding of key processes driving changes in carbon storage. Earth system models offer a quantitative framework for interpreting glacial biogeochemical changes in terms of their implications for carbon cycling and proxy evolution in a dynamic, 3-dimensionally resolved ocean. These models are built on the same chemical principles (carbonate system solvers, Redfield ratios, etc.) as the conceptual models underlying the above-mentioned quantitative methods and are tuned to reproduce observed spatial biogeochemical gradients of the present-day ocean. In the absence of observational data sets spanning glacial-interglacial time scales or suitable reconstructions of past conditions, Earth system models can provide physical and chemical constraints on scenarios of carbon cycle changes and allow for testing the robustness of conceptual models that rely on spatial or local data for examining temporal and global changes. A key advantage of employing Earth system models is their capacity to consider spatial heterogeneity, including tracer transport by ocean circulation, the exchange of organic and inorganic carbon and nutrients with ocean sediments, and related imbalances between weathering fluxes to the ocean and sedimentary burial (Tschumi et al., 2011). For instance,

previous modelling studies have shown that AOU is not a reliable proxy of regenerated carbon in the deep ocean (Cliff et al., 2021; Schmittner & Fillman, 2024), and that the relationship between water mass age and DIC content is basin-specific and variable over glacial-interglacial timescales (Kurahashi-Nakamura et al., 2022).

Here, we build upon this methodological foundation by testing empirical approaches for reconstructing the glacial carbonate system based on reconstructed carbon cycle metrics. We assess the predictive skill of DIC estimates from  $\text{CO}_3^{2-}$  (Section 3.1), and from  $\text{O}_2$  or  $\delta^{13}\text{C}$  (Section 3.2), using idealized, factorial simulations where only a single process forcing is changed. We then evaluate proxy-based predictions in transient glacial-interglacial simulations (Section 3.3). Finally, we discuss the extent to which changes in DIC can constrain past atmospheric  $\text{CO}_2$  levels.

## 2. Methods

We use simulations with the Earth system model of intermediate complexity Bern3D v2.0. The model uses MOCSY v2.0 (J. Orr & Epitalon, 2015) to simulate carbonate system changes, which is a best-practice carbonate system solver that is also used in several General Circulation Models (GCMs). Importantly, this means that Bern3D is not a different carbonate system model, but uses the same carbonate system solver that is commonly applied in other Earth system models and performs similarly to those used in the interpretation of proxy records, for example, CO2SYS (Humphreys et al., 2022; J. Orr & Epitalon, 2015). Bern3D projects the well-understood ocean box model carbonate chemistry into a spatially heterogeneous ocean with dynamic circulation, sea ice, and biogeochemical tracer exchange not only with the atmosphere, but also with ocean sediments and the lithosphere, while remaining computationally-efficient enough to simulate transiently climate-carbon cycle changes over repeated glacial cycles. Additional information about the model is provided in Appendix A.

Bern3D also includes diagnostic tracers for preformed DIC and phosphate, which track the fractions of DIC and phosphate that leave the ocean's surface without being incorporated into marine organic carbon by surface ocean production. Regenerated DIC and phosphate are then calculated as the difference between total and preformed concentrations, and include the weathering-burial imbalance when sediment dynamics are included in a simulation. Atmosphere-ocean gas exchange and carbonate chemistry are simulated according to the OCMIP-2 protocols (Najjar et al., 1999; J. Orr et al., 1999; J. C. Orr et al., 2017; J. Orr & Epitalon, 2015; Wanninkhof, 2014). Bern3D tracks the theoretical  $\text{O}_2$  concentration of water in an abiotic ocean ( $\text{O}_{2,\text{sol}}$ ), for example, without the life-time effects of primary production and organic matter remineralization in the water column or sediments in simulations with interactive sediments). In our analysis, we can therefore calculate  $\text{O}_2$  physically and biologically driven disequilibria in the surface ocean (see Appendix A) in addition to Apparent Oxygen Utilization (AOU, i.e. the dissolved  $\text{O}_2$  at equilibrium with the atmosphere minus the actual dissolved  $\text{O}_2$ ) to discount  $\text{O}_2$  changes due to air-sea flux changes for analytical purposes.

Bern3D presents a “best case scenario” for many of the assumed linear relationships between carbon cycle proxies and DIC, because the Bern3D model does not include some processes that cause uncertainty in real world applications, for example, variable Redfield ratios and rain ratios, while still accounting for more processes and spatial complexity than box models. Therefore, some correlations that exist in the model could still break in reality due to effects of these processes missing in the model. Yet, any correlation found not to be robust in this model, with its additional sophistication over box models and conceptual models, is unlikely to exist in the real world.

In this spirit, we test how well DIC changes can be reconstructed under different forcings and in different ocean regions from different combinations of tracers that could be obtained from proxy records in Bern3D simulations. For this, we take simulated (a)  $\text{CO}_3^{2-}$ , (b) the simulated combination of  $\text{CO}_3^{2-}$  and pH, in combination with known temperature and salinity, (c)  $\delta^{13}\text{C}$  and AOU from the simulations as perfect proxy records. Simulated DIC is the target to be reconstructed from these computed “proxy records.” We analyze the results from two sets of experiments: (a) step-wise changes in selected processes and (b) orbital changes over the last glacial cycle in a recently published simulation ensemble of transient glacial-interglacial carbon cycle changes (Adloff, Jeltsch-Thömmes, et al., 2024a, 2024b, see also Appendix A). In these simulations, we investigate the conditions under which metrics and postulated relationships work and fail, and test the robustness of the resulting quantitative estimates. This provides a relevant new model perspective to further develop the interpretative framework required to quantitatively constrain glacial carbon cycle dynamics from proxy records.

**Table 1**  
*Step-Change Experiments in Simulation Set A*

ID	Forcing
Cooling	Radiative forcing $-9 \text{ W/m}_2$
Hosing	0.2 Sv freshwater forcing in North Atlantic
PIC:POC	$2/3 \times \text{PIC:PIC}$
Remin	Deepening of mean remineralization depth

Experiment set A is a series of step changes in selected processes, that were applied to the pre-industrial steady state and run to equilibrium over 100 kyr. We selected the following processes, which were previously found to be relevant for glacial-interglacial carbon cycle changes (Table 1): “Cooling”—global cooling of  $\sim -7.5^\circ\text{C}$  (radiative forcing of  $-9 \text{ W/m}_2$ ), “Hosing”—a  $\sim -9 \text{ Sv}$  Atlantic Meridional Overturning Circulation (AMOC) weakening, achieved by applying a freshwater forcing of 0.2 Sv in the North Atlantic ( $45\text{--}70^\circ\text{N}$ ), “PIC:POC”—lowered PIC:POC ratio (reduction by 1/3) and “Remin”—a lowering of the mean remineralization depth by altering the remineralization profile in the upper 2000 m of the water column as shown in

Figure S20 in Supporting Information S1. We produced these simulations to study processes rather than attempting a realistic simulation of the last glacial. Hence, the scaling of each forcing is arbitrary within a range that is roughly consistent with Earth system changes of the last glacial cycle.

The step changes in the selected forcings or model set-ups in the first simulation set allow for probing the response in terms of magnitude and timescales, as in a linear (or approximately linear) system, the resulting Green's function fully characterizes the system's response to any change. We use this to understand the model behavior, that is, the processes that drive temporal changes in different carbonate system tracers. The process-specific simulations thus provide the opportunity to systematically test the effects of various Earth system processes on metrics characterizing the carbonate system, the biological pump, DIC and atmospheric  $\text{CO}_2$  in a closed (excluding exchange with sediments and lithosphere) and open atmosphere-ocean system. We then use the transient simulations of a full glacial cycle in experiment set B to understand how these processes would have affected the skill of DIC reconstruction methods in an ocean that transitions through glacial changes.

Experiment set B is an already published set of transient experiments described in detail in Adloff, Jeltsch-Thömmes, et al. (2024a, 2024b). Starting from an interglacial spin-up with the orbital configuration of MIS19, we used the temporal evolution of either Antarctic ice core  $\delta\text{D}$  (Jouzel et al., 2007) or benthic  $\delta^{18}\text{O}$  (Lisiecki & Raymo, 2005) to simulate the effect of varying strength of different Earth system processes over the last eight glacial cycles, specifically, glacial-interglacial change in physical climate and AMOC strength, Southern Ocean gas exchange efficiency, Southern Ocean wind forcing, organic matter remineralization rate, ratio of organic to inorganic particle export, whole ocean nutrient inventory, land carbon storage and external alkalinity fluxes (Table A1). We re-analyze the results of these experiments for the last glacial cycle here because they broadly represent the range of proposed, potential physical, and biogeochemical mechanisms of glacial-interglacial carbon cycle changes in factorial simulations.

In both experiment sets, the simulations were run once with and once without interactive sediments. Loss fluxes to the lithosphere in simulations with interactive sediments are compensated for at pre-industrial equilibrium by a corresponding input flux from weathering that is kept constant throughout all experiments with interactive sediments.

All of our simulations contain the direct response to a forced change in a distinct process, as well as the ensuing cascade of processes that further evolve the carbonate system over time, given the coupled nature of the atmosphere-ocean-sediment-lithosphere biogeochemical system. A detailed description of our simulation ensembles is provided in Appendix A.

### 3. Results

#### 3.1. Predicting DIC From $\text{CO}_3^{2-}$

A body of theoretical and observation-driven research has developed approaches to reconstruct changes in DIC from changes in  $\text{CO}_3^{2-}$ . Yu et al. (2016) showed that spatial  $\text{CO}_3^{2-}$  variations in the deep Atlantic linearly correlate with the difference between total alkalinity (from now on ALK) and DIC in observations and model simulations of pre-industrial and glacial steady state runs in the UVic and LOVECLIM models:

$$\Delta\text{CO}_3^{2-} = k \times (\Delta\text{ALK} - \Delta\text{DIC}) \quad (1)$$

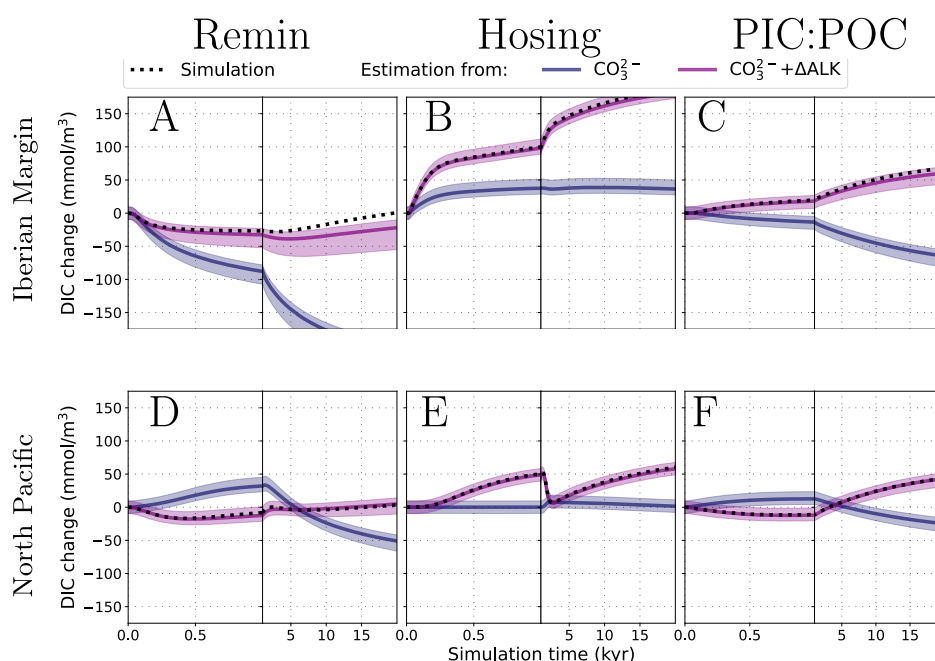


**Figure 1.** Dissolved inorganic carbon (DIC) change predicted from  $\text{CO}_3^{2-}$  (blue) and from the combination of  $\text{CO}_3^{2-}$  and ALK (purple) versus true (simulated) DIC change (black dashed). Results are for benthic DIC in the Iberian Margin (top) and the North Pacific (bottom) and from Bern3D simulations with a step change at time zero (see Appendix A) in the remineralization profile of organic matter (Remin), the particulate inorganic to particulate organic carbon export (PIC:POC), and fresh water hosing into the North Atlantic causing a strong reduction in Atlantic Meridional Overturning (Hosing). DIC is predicted by assuming a linear relationship between DIC and  $-1/k \times \text{CO}_3^{2-}$  (i.e., assuming no influence from changing alkalinity, as often done in proxy interpretations; blue line) or assuming a linear relationship between DIC and  $-1/k \times \text{CO}_3^{2-} - \text{ALK}$  (i.e., with knowledge of alkalinity change, purple line). The uncertainty interval around the predicted changes ( $k = 0.59$ ) spans proportionality constants  $k$  between 0.53 and 0.60 and an assumed analytical uncertainty of  $1\sigma = 5.0 \text{ mmol/m}^3$  for  $\text{CO}_3^{2-}$  (when derived from B/Ca of benthic foraminifera, Yu & Elderfield, 2007; Yu et al., 2013). Shown are the simulations that include weathering-burial imbalances. We repeated the same comparison in simulations without weathering-burial imbalances (Figure S2 in Supporting Information S1) and for additional ocean regions (Figure S1 in Supporting Information S1). Coordinates for the example locations are provided in Table A2.

with a proportionality constant  $k$  between 0.53 and 0.59. In the Bern3D model employed here, the same spatial relationship prevails in the pre-industrial Atlantic, and  $k$  varies between 0.54 – 0.66 in the Atlantic over simulated past glacial cycles, even considering a wider range of biogeochemical perturbations than in previous modeling studies (Appendix C). If this spatial correlation can be equated to a temporal correlation, this relationship would allow inference of temporal DIC difference from the corresponding  $\text{CO}_3^{2-}$  difference, if the ALK change is known or assumed. Here, we assume constant ALK, which is often done in practice (e.g., Farmer et al., 2019; Yu et al., 2016, 2023), and compare it to the hypothetical case that the actual ALK change was known, in order to estimate the error introduced by the assumption of constant ALK.

Figure 1 shows the simulated (black curve) and inferred (colored curves) benthic DIC changes under three forcings and in two different oceanographic settings (two more—the benthic Eastern Equatorial Pacific and the Atlantic sector of the Southern Ocean—are shown in Figure S1 in Supporting Information S1). The DIC estimate based on  $\text{CO}_3^{2-}$  alone (with assumed constant ALK, blue lines) deviates in almost all cases from the actual simulated DIC change in amplitude and often also in sign. Crucially, these errors appear despite Bern3D showing the same spatial correlations in the benthic carbonate system as determined in GLODAP (Appendix C). In this case, we overestimate DIC changes in the scenario of a deepening of the mean remineralization depth (Figures 1a and 1d), underestimate DIC change in the scenario of a hosing-induced AMOC weakening ( $\sim 9 \text{ Sv}$ , Figures 1b and 1e) and predict a DIC change of the wrong sign in the case of lowering the PIC:POC of export production by one third (Figures 1c and 1f). Our results imply that DIC changes can in general not be predicted from  $\text{CO}_3^{2-}$  data only.



The mismatch between predicted and true DIC arises from neglecting ALK changes. Knowledge of ALK, which is typically not available from proxy reconstructions, would allow for better predicting DIC. This is illustrated by the very good matches between DIC predicted from  $\text{CO}_3^{2-}$  and ALK and simulated DIC (purple vs. black in Figure 1). The simulated ALK changes are caused by ALK redistribution within the ocean due physical transport and biological activity and changes of the overall marine ALK inventory (for a detailed exploration see Appendix B).

Uncertainty in the value of the proportionality constant  $k$ , which is empirically determined from a spatial correlation between (ALK-DIC) and  $\text{CO}_3^{2-}$  (which varies between ocean basins) and applied to temporal changes (Farmer et al., 2019; Yu et al., 2016, 2019, see SI Appendix C for an exploration in Bern3D), is a minor error source (purple shading and difference between purple and black lines in Figure 1). However, there are specific locations and forcing scenarios where  $k$  becomes a larger error source (Figure S15 in Supporting Information S1, Appendix C), for example, below the oxygen minimum zone in the East Equatorial Pacific (Figure S1 in Supporting Information S1).

In simulations without weathering-burial imbalances (i.e., atmosphere-ocean only, Figure S2 in Supporting Information S1) ALK changes are smaller. Thus, the direction of DIC change is correctly determined from  $\text{CO}_3^{2-}$  alone in the case of changing remineralization rate and hosing, but not for changes in PIC:POC. Yet in these simulations, amplitude errors also exist in almost all cases. Independent of whether weathering-burial imbalances are considered in our simulations or not, in all tested scenarios and regions errors become apparent as soon as DIC changes  $>10 \text{ mmol/m}^3$  evolve, as early as 100 years after the perturbation, and in most cases further increase throughout the simulations (Figure 1). These results imply that a quantitative reconstruction of DIC from  $\text{CO}_3^{2-}$  alone is generally not possible both on short (decadal-to-century) and long timescales. Given a-priori unknown local ALK changes, a second carbonate system constraint is required for a more accurate solution of the carbonate system. Previous studies discussed the use of pH as a constraint, given that it is the only other carbonate system parameter that can be reconstructed directly from proxy data (J. W. Rae et al., 2011; Yu et al., 2010). In principle, the carbonate system can be solved and DIC change quantified if  $\text{CO}_3^{2-}$ , pH, temperature and salinity changes are known from perfect, independent proxies, but the close correlation between pH and  $\text{CO}_3^{2-}$ , in combination with uncertainties in proxy-data and in carbonate system equilibrium constants, introduce large uncertainty in the estimated DIC (J. W. Rae et al., 2011; J. W. B. Rae, 2018).

### 3.2. Predicting DIC Changes From $\text{O}_2$ Utilization or $\delta^{13}\text{C}$

Next, we test the prediction of the simulated DIC changes from simulated changes in  $\delta^{13}\text{C}$  by assuming that organic matter remineralization releases C with a  $\delta^{13}\text{C} = -24\text{‰}$  and from simulated  $\text{O}_2$  utilization by multiplying simulated AOU with the model specific Redfield ratio of organic matter ( $\text{DIC}:\text{O}_2 = 117:170$ ).

Air-sea disequilibria of  $\text{CO}_2$  in regions with deep water formation increase marine carbon storage (Nowicki et al., 2024; Schmittner & Fillman, 2024), a process which might have been amplified during glacial times (Khaliwala et al., 2019). Air-sea disequilibria in areas of deep water formation also exist for  $\text{O}_2$  and  $\delta^{13}\text{C}$  (Ito et al., 2004; Khaliwala et al., 2019; Omta et al., 2024), but the timescales for bringing the surface mixed layer  $\text{O}_2$  ( $<1$  year),  $\text{CO}_2$  ( $\sim 1$  year) and  $\delta^{13}\text{C}$  ( $\sim 10$  years) in equilibrium with the atmosphere by air-sea gas exchange differ. Further, if these disequilibria get incorporated into deep water, they do not follow an assumed Redfield ratio for organic matter (Cliff et al., 2021; Schmittner & Fillman, 2024). In the case of climate-driven changes to these equilibria, measuring AOU or  $\delta^{13}\text{C}$  changes in deep water masses does not provide a robust quantitative constraint on the amount of DIC released during organic matter remineralization, despite the close link of  $\text{O}_2$ ,  $\delta^{13}\text{C}$  and DIC in the remineralization processes (see Cliff et al., 2021; Schmittner & Fillman, 2024, and Appendix D). Hence, AOU or  $\delta^{13}\text{C}$  are not perfect direct tracers of DIC derived from remineralization ( $\text{DIC}_{\text{org}}$ ) in the deep ocean in scenarios of climate change. Here, we explore the correlation between AOU,  $\delta^{13}\text{C}$  and total DIC change, which is caused by changes in remineralization (i.e.,  $\text{DIC}_{\text{org}}$ ),  $\text{CaCO}_3$  dissolution, surface ocean disequilibria and weathering-burial imbalances.

At the Iberian margin and for scenario “Remin” with a sudden deepening of the mean remineralization depth (Figure 2a), the benthic DIC decrease is underestimated by AOU (Figure 2a) because AOU does not capture the reduction in  $\text{CaCO}_3$  dissolution due to reduced export production (see section Appendix B). AOU is, nevertheless,

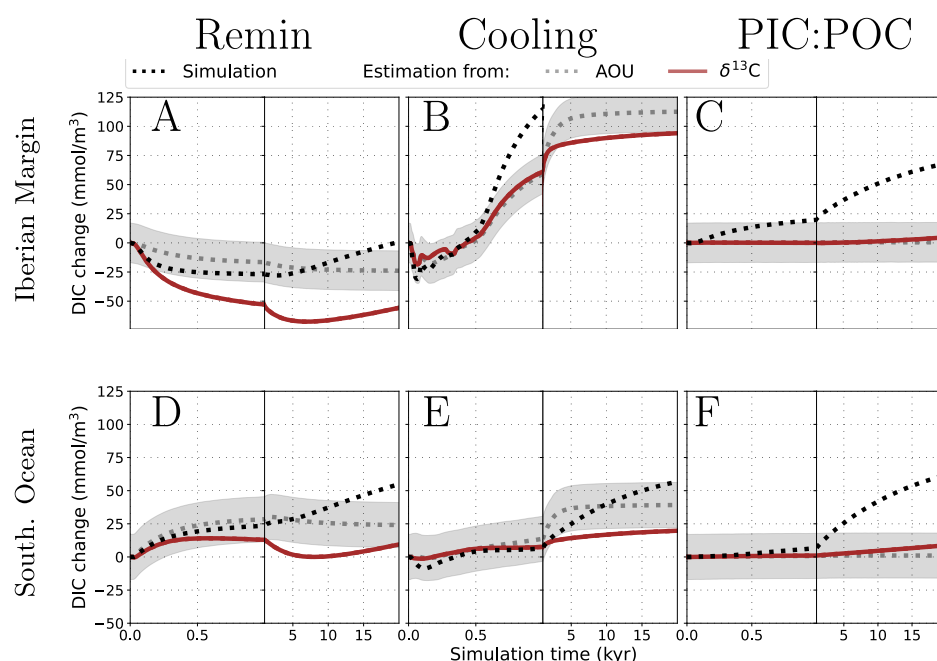


**Figure 2.** Simulated and predicted benthic dissolved inorganic carbon (DIC) changes due to step changes in various processes in different oceanographic settings. The simulated DIC changes (black dashed line) are compared to the DIC changes predicted from simulated apparent oxygen utilization and  $\delta^{13}\text{C}$  changes. The step change in the forced process occurs at time zero. Shown are the simulations that include weathering-burial imbalances. We repeated the same comparison in simulations without weathering-burial imbalances (Figure S6 in Supporting Information S1) and in other settings (Figure S5 in Supporting Information S1).

a good proxy of  $\text{DIC}_{\text{org}}$  (Appendix D) at the Iberian margin and for scenario “Remin.” Predicted DIC from  $\delta^{13}\text{C}$  is also insensitive to changes in the hard tissue pump over  $\sim 1$  kyr (“PIC:POC” scenario, Figures 2c and 2f, red line). Yet, the  $\delta^{13}\text{C}$  prediction overestimates the decrease in local  $\text{DIC}_{\text{org}}$  (Figure D1) and DIC (Figure 2a, red vs. black dotted lines) in the “Remin” scenario. This prediction error is caused by fractionation changes during export production (the strong reduction of  $\text{pCO}_2$  in the surface ocean in scenario “Remin” causes  $\delta^{13}\text{C}$  of POC to increase Jeltsch-Thömmes et al. (2019) by about 2‰) and POC burial changes in marine sediments which alter the isotopic signature of the local water masses in addition to the changed amount of local remineralization.

In the scenario of a sudden cooling of the Earth system (“Cooling”), both AOU and  $\delta^{13}\text{C}$  overestimate the resulting  $\text{DIC}_{\text{org}}$  change at the Iberian Margin (Figure D1), because local  $\text{O}_2$  and  $\delta^{13}\text{C}$  also change due to an increased presence of Southern-sourced water, which contains a larger signal of surface ocean disequilibrium in both tracers (for more detail, see Appendix D). While AOU and  $\delta^{13}\text{C}$ -derived  $\text{DIC}_{\text{org}}$  compare poorly to the simulated  $\text{DIC}_{\text{org}}$  in our simulation, they compare better to the simulated total DIC change (Figures 2b and 2e), at least over the first 500 years of our simulations, despite the contributions of water mass replacement and hard tissue pump changes that AOU and  $\delta^{13}\text{C}$  cannot predict. Thus, while AOU and  $\delta^{13}\text{C}$  do not accurately track the processes behind the DIC changes in this scenario of cooling, they contain information about the direction and order of magnitude of the initial DIC shift. After 500 years, AOU and  $\delta^{13}\text{C}$  change at a slower pace than DIC at the Iberian Margin in this cooling scenario, causing an increasing mismatch between predicted and simulated DIC.

Beyond the first 1 kyr of our step change experiments, the predictability of total DIC changes from AOU and  $\delta^{13}\text{C}$  changes decreases further. Carbonate compensation and weathering imbalances, which alter preformed DIC in the ocean, are not or only poorly tracked by these metrics, and the adjustment of the marine  $\delta^{13}\text{C}$  distribution to the new carbon cycle state is complex and spatially heterogeneous—and keeps changing beyond the re-distribution of DIC (Jeltsch-Thömmes & Joos, 2020).

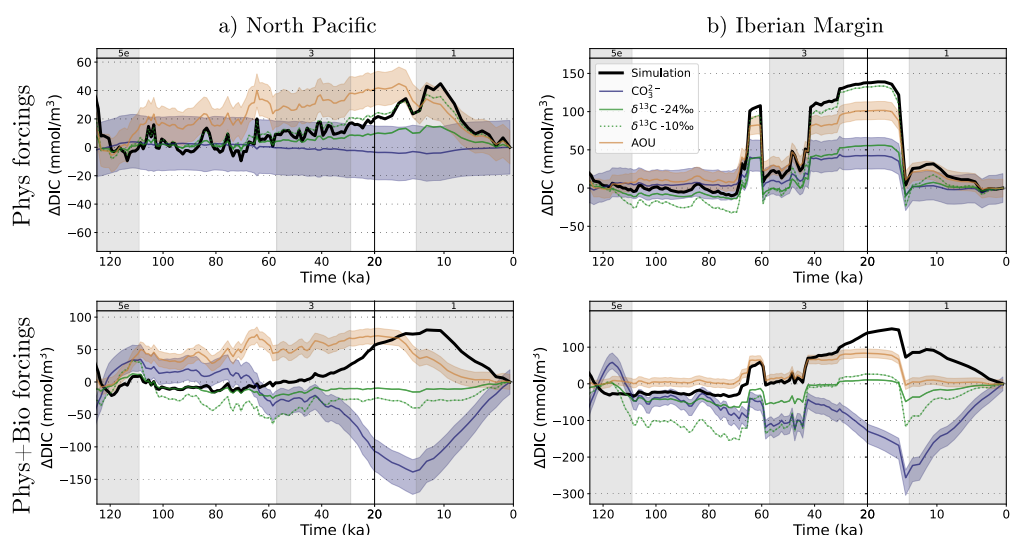


**Figure 3.** Temporal changes in simulated (black) and estimated dissolved inorganic carbon (DIC) from  $\text{CO}_3^{2-}$  (blue),  $\delta^{13}\text{C}$  (green, assuming a  $\delta^{13}\text{C}$  of  $-24\text{‰}$  or  $-10\text{‰}$ ) and apparent oxygen utilization (orange) for a simulation of repeated orbitally-paced physical forcing (simulation PHYS from Adloff et al. (2024a, 2024b), top row) and a simulation with additional biogeochemical forcings (simulation ALL from Adloff et al. (2024a, 2024b), bottom row). The shading around estimated DIC curves show propagated analytical uncertainties ( $\text{CO}_3^{2-}$ : 5.0 mmol/m<sup>3</sup>,  $\text{O}_2$ : 17 mmol/m<sup>3</sup>,  $\delta^{13}\text{C}$ : 0.2‰). Results are for benthic grid cells at the Iberian Margin and in the North Pacific. Gray bars indicate uneven Marine Isotope Stages.

These results demonstrate that the prediction of DIC and  $\text{DIC}_{\text{org}}$  from AOU or  $\delta^{13}\text{C}$  can be in substantial error on both short and long timescales. The magnitude and sign of the mismatch depends on location, process forcing, and time evolved since the perturbation in these factorial step change simulations.

### 3.3. Predicting DIC From Carbonate System Proxies: Results of Transient Glacial-Interglacial Simulations

The idealized, factorial step-change simulations with a single change discussed thus far are informative but proxy records reflect the combination of different time evolving processes. During past glacial cycles changes of ocean circulation and marine biogeochemistry, such as shifts in the mean remineralization depth and export production, have occurred transiently, alongside and in response to each other, creating a much more complex scenario.

Figure 3 compares DIC predictions based on  $\text{CO}_3^{2-}$ , AOU and  $\delta^{13}\text{C}$  to the actually simulated DIC changes over the last glacial cycle in two simulations (Appendix A) with continuous orbitally-paced forcing of the open atmosphere-ocean-sediment system in Bern3D: one simulation including only physical forcings (insolation, aerosol- and greenhouse gas-related temperature changes, Southern Ocean wind forcing changes) and one with additional changes in biogeochemistry (remineralization depth, nutrient input, PIC:POC ratio, land carbon storage). Results are shown for the deep North Pacific and Iberian Margin in Figure 3 and for additional locations in Figure S7 in Supporting Information S1. Both simulations reproduce reconstructed salinity and temperature changes at the Iberian Margin (Duplessy et al., 1991) and an AMOC strength reduction to 11 Sv, compared to a proxy-constrained range of 10–12.5 Sv during glacial maxima (Pöppelmeier et al., 2023). Yet, the first simulation (upper row in Figure 3) can be seen as a minimal forcing case for carbon cycle changes over the last glacial cycle because it does not include changes to the whole-ocean nutrient inventory, remineralization curve, rain ratio and terrestrial carbon release while the second (bottom row of Figure 3) does (see SI Appendix A, Adloff, Jeltsch-Thömmes, et al., 2024a, 2024b). Here, we test how well the simulated DIC changes, resulting from a complex interplay of different Earth system changes, can be estimated with the tested methods from internally consistent model output.

Figure 3 shows that even in a simulation with minimal glacial-interglacial forcing and thus weathering-burial imbalances (top row), the sign and amplitude of the reconstructed DIC changes are inaccurate for large parts of the time series. In a separate simulation without weathering-burial imbalances, the empirical relationship



between DIC and  $\text{CO}_3^{2-}$  (blue lines) constrains well the direction of DIC change in several locations that we tested (e.g., in Figure S8 in Supporting Information S1). Yet, the assumption of constant local ALK causes an error in the amplitude of the estimated DIC changes of up to 50%, well outside the analytical uncertainty also in that simulation because of local ALK changes due to ALK re-distribution (Figure S9 in Supporting Information S1).

As previously discussed, AOU and  $\delta^{13}\text{C}$  are imperfect tracers of  $\text{DIC}_{\text{org}}$  because they track other  $\text{O}_2$  and  $\delta^{13}\text{C}$  fluxes in addition to those resulting from soft tissue pump changes. Large errors might thus be expected when estimating total DIC change from AOU or  $\delta^{13}\text{C}$ , given that total DIC change is the sum of DIC changes associated with the soft tissue pump and those resulting from hard tissue pump and solubility changes. However, we find that AOU and  $\delta^{13}\text{C}$  can predict total DIC change better than  $\text{CO}_3^{2-}$  in some settings and scenarios, especially at glacial maxima (Figure 3, upper row). The reason for this is that the processes that cause errors in the prediction of  $\text{DIC}_{\text{org}}$  changes from AOU and  $\delta^{13}\text{C}$  also affect total DIC. For example, AOU is influenced by both remineralization and biological disequilibrium changes and therefore constrains total DIC change in settings and scenarios where these two processes dominate the DIC change (Appendix D). Likewise,  $\delta^{13}\text{C}$  is controlled by circulation and fractionation changes in addition to changes of the soft tissue pump (see Section 3.2). The fact that the error of the DIC reconstruction from  $\delta^{13}\text{C}$  is reduced in some locations and time intervals by assuming an “effective” isotopic signature of added or removed DIC i.e. lower (e.g.,  $\delta^{13}\text{C} = 10\text{‰}$ , Figure 3) than typical values of organic matter (e.g.,  $\delta^{13}\text{C} = 24\text{‰}$ ), suggests that inorganic processes overprint on the relationship between  $\delta^{13}\text{C}$  and DIC change in the soft tissue pump.

In simulations with strong biogeochemical perturbations (Figure 3, lower row), errors in DIC changes reconstructed from  $\text{O}_2$  utilization or  $\delta^{13}\text{C}$  changes are large due to sediment changes, and none of the tested methods provide a reliable metric of total DIC change. Similarly, all three methods fail to track DIC changes in scenarios where DIC change is predominantly driven by ALK change (Figure S19 in Supporting Information S1).

## 4. Discussion

### 4.1. The Role of ALK Changes for the Reconstruction of Glacial-Interglacial DIC Changes

The uncertainty in local ALK change is the determining factor for the accuracy of DIC estimates based on carbonate system reconstructions. Considering ALK changes is easy in our theoretical study, because ALK is explicitly traced and part of the model output. ALK is notoriously difficult to reconstruct in the real world, due to the lack of a readily available ALK proxy. In the absence of proxy data, a common reasoning for the assumption of constant local ALK is that the typical timescale of carbonate compensation (multiple millennia) implies little ALK variability on shorter time scales (e.g., W. S. Broecker & Peng, 1987; Yu et al., 2023). However, slow global ALK changes due to carbonate compensation do not preclude faster local ALK changes (Figure S3 in Supporting Information S1). In our simulations with interactive sediments, carbonate compensation restores global  $\text{CaCO}_3$  burial rates to match marine ALK inputs on typical time scales of multiple millennia and in the process creates persistent local ALK changes by moving the carbonate compensation depth. Yet, changes in ocean circulation and the biological pump re-distribute ALK on all time scales (including decadal to millennial, see Appendix B and Table S1 in Supporting Information S1), even if the global ALK reservoir remains constant. Such ALK changes affect the evolution of local  $\text{CO}_3^{2-}$  and DIC in all our step change experiments. This reduces the predictability of DIC from  $\text{CO}_3^{2-}$  also in experiments without carbonate compensation (Figure S2 in Supporting Information S1). Without constraints on the local ALK change, the observed spatial correlation in the deep Atlantic between  $\text{CO}_3^{2-}$  and DIC (Yu & Elderfield, 2007) does therefore also not *a-priori* constrain local DIC changes over time.

Earth system models may be used to understand possible magnitudes and directions of local and global ALK changes in response to specific forcing scenarios, but the validity of absolute simulated ALK changes depends entirely on the accuracy of the model and forcing scenario. In our simulations, the amplitude and direction of the glacial-interglacial alkalinity change depends strongly on the forcing (glacial-interglacial alkalinity changes span  $-50 - +120 \text{ mmol/m}^3$  in the global,  $-50 - +180 \text{ mmol/m}^3$  in the surface and  $-50 - +90 \text{ mmol/m}^3$  at the bottom of the ocean (global mean) across our simulations) and is spatially heterogeneous (Figure S16 in Supporting Information S1).

Local ALK changes can occur due to a range of processes. Changing the efficiency of the biological pump or the ratio of organic to inorganic particle export from the euphotic zone cause the largest alkalinity changes at all depths in our simulations. Changes in the flux and composition of biogenic particles reaching the deep ocean can also cause negative local and global ALK changes during glacial cycles (Figure S17 in Supporting Information S1).

Water mass replacements can cause sudden and large ALK shifts locally (Figure 1). For example, at the Iberian Margin, most of the simulated glacial-interglacial ALK shift ( $\Delta\text{ALK} = 90 \text{ mmol/m}^3$ ) occurs due to sudden shifts of AMOC states, in abrupt jumps shorter than 1000 years. The large and fast variability of ALK in the North Atlantic due to AMOC changes has also been found with other models, for example, Lacerra et al. (2017) who simulated benthic ALK changes between  $20 - >80 \text{ mmol/m}^3$  over 2.5 kyr after an AMOC shutdown, not including interactions with marine sediments. While the timing and magnitude of circulation change are model and scenario dependent, and likely not accurate in our simplified simulation, advection of ALK needs to be considered when investigating local ALK changes. In all simulations, and irrespective of whether interactive sediments are included or not, local ALK changes can occur as fast as DIC changes.

Similar conclusions on ALK changes can be drawn from other model studies. Proxy-constrained ( $\text{CO}_2$ ,  $\delta^{13}\text{C}$ ,  $\Delta^{14}\text{C}$ ) deglacial circulation changes in an ocean-atmosphere only model yielded glacial-interglacial ALK changes in all ocean basins, with the largest in the deep Atlantic ( $\sim 20 \text{ mmol/m}^3$ ) and the smallest in the Indo-Pacific (a few  $\text{mmol/m}^3$ ) (Kobayashi et al., 2024). In ocean-atmosphere-sediment models, local ALK changes can be smaller, as large, or larger than local DIC changes (see also Table S2 in Supporting Information S1 for results of our simulations). In Brovkin et al. (2007)'s experiments, which used forcings chosen for a realistic representation of the LGM climate and carbon cycle, global mean glacial-interglacial ALK changes are as big as those of global mean DIC when sea level or land carbon change are considered, and bigger when temperature, circulation and shallow water carbonate deposition changes are additionally taken into account. Including all processes they tested, they simulated a global mean ALK difference of  $+257 \text{ mmol/m}^3$  between the LGM and Holocene states, of which  $71 \text{ mmol/m}^3$  were the result of sea level change. Kurahashi-Nakamura et al. (2022) provided a lower estimate of  $40\text{--}80 \text{ mmol/m}^3$  global mean ALK addition to the glacial ocean on top of the sea level effect needed to optimize their model-data metric.

The exact scale of global marine ALK inventory changes due to imbalances in the geologic carbon cycle has for several decades been the matter of ongoing debate (Börker et al., 2020; Boyle, 1992; de Souza et al., 2022; Frings, 2019; Jones et al., 2002; Sigman & Hain, 2024; Von Blanckenburg et al., 2015) and to our knowledge no consensus has yet been reached. Cartapanis et al. (2018) estimated ALK variations of up to  $150 \text{ mmol/m}^3$  in the global mean across the last glacial cycle from reconstructions of marine  $\text{CaCO}_3$  burial rates assuming constant ALK inputs. Combining this estimate with estimates of terrestrial weathering change during the last deglaciation, Kurahashi-Nakamura et al. (2022) estimated that the ocean could have lost  $0.5\text{--}1.0 \cdot 10^{17} \text{ mol}$  equivalents over that period, roughly  $37\text{--}75 \text{ mmol/m}^3$ . Yu et al. (2019) estimated that global mean ALK was  $80\text{--}120 \text{ mmol/m}^3$  higher at the LGM than today by assuming that all carbon missing from atmosphere and land at the LGM were stored as DIC in the ocean and neutralized by carbonate compensation. Locally, several studies argued for glacial-interglacial ALK changes, at least regionally, based on  $\text{CO}_3^{2-}$  records (e.g., Kerr et al., 2017; Rickaby et al., 2010; Yu et al., 2013) but the assumption of constant ALK, at least before carbonate compensation, is still often made in the interpretation of  $\text{CO}_3^{2-}$  in other instances (e.g., Farmer et al., 2019; Yu et al., 2016; Yu et al., 2023).

Our analysis strongly suggests that DIC estimates are currently best achieved through a combination of proxy data and dynamic ocean and Earth system modeling, as we lack sufficient observational records to validate methods for reconstructing temporal DIC and ALK changes in the real world, and the simple empirical relationships currently used are found to have substantial shortcomings. While Earth system models are simplified representations of reality and do not provide definite answers, they provide a powerful and internally consistent tool for testing conditions and processes to translate proxy-derived  $\text{CO}_3^{2-}$  or pH to DIC. Ideally, Earth System model results should be constrained by a broad range of different high-quality proxy data in probabilistic approaches (Jeltsch-Thömmes et al., 2019; Pöppelmeier et al., 2023) to improve the certainty of their simulated DIC and ALK changes.

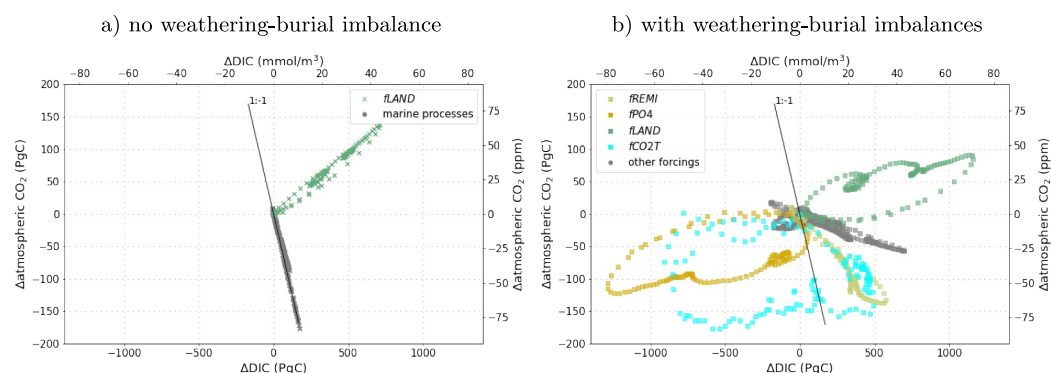


**Figure 4.** Correlation between global marine dissolved inorganic carbon and atmospheric  $\text{CO}_2$  changes over the last glacial cycle (120 ka–PI) without (a) and with (b) interactive sediments.

#### 4.2. Deep Ocean DIC Change Does Not Uniquely Constrain Changes in Atmospheric $\text{CO}_2$

Assuming that we had a reliable method to reconstruct global DIC change, the question arises how this relates to changes in atmospheric  $\text{CO}_2$ . Is it possible to quantify the role of marine carbon storage in glacial-interglacial atmospheric  $\text{CO}_2$  changes based on reconstructed DIC?

In a closed atmosphere-ocean system, any marine process that increases total DIC reduces atmospheric  $\text{CO}_2$  by an equivalent amount. Terrestrial carbon release during glacial phases causes a larger long-term change in DIC storage than atmospheric  $\text{CO}_2$  as the carbonate system buffers  $\text{CO}_2$  uptake and ocean circulation mixes C into the ocean's interior (Jeltsch-Thömmes & Joos, 2020; Kheshgi, 2004; Lord et al., 2016).

When considering an open atmosphere-ocean-sediment system, the total inventory of carbon of the atmosphere, ocean, and land biosphere is not preserved and the relationship between atmospheric  $\text{CO}_2$  and DIC changes depends on the sediment perturbation. In most simulations, there is still a linear negative correlation between atmospheric  $\text{CO}_2$  and DIC changes (“other forcings” in Figure 4) but with a much weaker slope, that is, DIC change is dominated by sedimentary rather than atmospheric carbon storage change. This is consistent with previous studies that concluded that substantially larger carbon storage changes in the ocean than in the atmosphere best reproduce proxy differences across the last deglaciation (Jeltsch-Thömmes et al., 2019; Morée et al., 2021). However, we also found processes for which there is no linear relationship between atmospheric  $\text{CO}_2$  and DIC change. For example, increased nutrient input ( $f\text{PO}_4$ ) or ALK supply ( $f\text{CO}_2\text{T}$ ) can even cause the coincidence of negative atmospheric  $\text{CO}_2$  and negative marine DIC anomalies at the LGM because of increased sedimentary POC and/or  $\text{CaCO}_3$  contents. While these processes cannot have dominated glacial-interglacial DIC changes because they produce benthic  $\delta^{13}\text{C}$  and  $\text{CO}_3^{2-}$  changes that are inconsistent with reconstructions (Adloff, Jeltsch-Thömmes, et al., 2024a, 2024b), they will have contributed to some degree to DIC changes in the real ocean. Given that sedimentary processes might have dominated benthic DIC changes on glacial-interglacial time scales and that these changes can be non-linearly related to atmospheric  $\text{CO}_2$ , it is a-priori unclear how a reconstructed DIC change in a given water mass at a given time relates to atmospheric  $\text{CO}_2$  change.

### 5. Conclusions

We investigated how well changes in ocean DIC can be estimated from reconstructions of carbonate ions ( $\text{CO}_3^{2-}$ ), AOU, or stable carbon isotope ratio ( $\delta^{13}\text{C}$ ) of DIC using published empirical relationships. To this end, we analyzed these quantities as simulated in a broad set of factorial simulations representing mechanisms of glacial-interglacial change. Predicting DIC from  $\text{CO}_3^{2-}$ , AOU, or  $\delta^{13}\text{C}$  results in large prediction errors. The existing empirical methods do not capture the interplay of the carbonate system, air-sea gas exchange, ocean circulation, biologically-mediated DIC and alkalinity re-distributions, and ocean-sediment exchange. Further, there is typically no clear relationship between changes in atmospheric  $\text{CO}_2$  and the total ocean inventory of DIC. Imbalances between the inputs of elements by weathering and losses by sedimentary burial cause large inventory changes in the coupled ocean-atmosphere system under glacial-interglacial forcing.

Specifically, we showed that temporal  $\text{CO}_3^{2-}$  changes can only be interpreted with a second carbonate system constraint because local ALK varies strongly due to re-distribution by the biological pump and ocean circulation, even when the total inventory of ALK in the ocean is constant. Constant local ALK can therefore not be assumed a-priori and does not provide an end-member either because it can in principle increase and decrease. In simulations with interactive sediments, sufficiently large sedimentary perturbations are simulated to significantly alter the global ALK inventory, even under a minimal glacial-interglacial forcing scenario. ALK changes over glacial cycle are also indicated by the limited variability of reconstructed benthic  $\text{CO}_3^{2-}$  in the Pacific and Indian Ocean over the last glacial cycle despite the postulated increase in marine C storage, which was attributed to large alkalinity changes (Yu et al., 2013; Zhang et al., 2022). Several studies address the uncertainty arising from unknown local ALK changes by adding quantitative information on biologically-mediated carbonate system change using AOU and  $\delta^{13}\text{C}$  to the interpretation of  $\text{CO}_3^{2-}$  reconstructions (Vollmer et al., 2022; Yu et al., 2008, 2019, 2020, 2022). Previous modeling studies showed that AOU is not a reliable predictor of  $\text{DIC}_{\text{org}}$  changes because it is to an unknown extent influenced by signals of biologically-driven and physically-driven air-sea disequilibria of  $\text{O}_2$  that do not correlate with the air-sea disequilibria of  $\text{CO}_2$  (Cliff et al., 2021; Khatiwala et al., 2019; Schmittner & Fillman, 2024). This is confirmed by our model results. Our results indicate that there are specific glacial-interglacial scenarios in which AOU and total DIC changes correlate and thus could possibly constrain DIC changes independently of the as-of-yet unconstrained ALK changes but it is unclear how well these scenarios capture real glacial-interglacial carbon cycle changes. These approaches require further investigations combining Earth system models and proxy data compilations.

$\text{CO}_3^{2-}$ , AOU and  $\delta^{13}\text{C}$  play an essential part in understanding glacial-interglacial carbon cycle dynamics and the carbon cycle response to large environmental change in general, and we strongly encourage further work and compilations of these records to increase their coverage, both in space and time. They are crucial for identifying the processes involved in glacial-interglacial carbon cycle changes and continue to challenge our conceptual understanding of carbon cycle dynamics (e.g., Anderson et al., 2019; Gottschalk et al., 2020; Kerr et al., 2017; Qin et al., 2017). They are also essential for benchmarking Earth system simulations, which otherwise have too many degrees of freedom to produce reliable glacial-interglacial carbon cycle changes. Here, we argued that the value of these records would be increased by using Earth system models for deriving quantitative information on DIC change than the often used conceptual models, which are valid in their underlying chemistry but do not contain the required complexity to provide robust estimates of carbon storage changes in the dynamic ocean.

## Appendix A: Detailed Methods

We analyze the simulation ensemble from Adloff, Jeltsch-Thömmes, et al. (2024a, 2024b). This ensemble was produced with the intermediate-complexity Earth system model Bern3D v2.0 (Edwards et al., 1998) which contains a 3D frictional-geostrophic ocean on a  $41 \times 40 \times 16$  grid with 22 prognostic and diagnostic tracers for physical circulation and marine biochemistry. Atmosphere-ocean gas exchange and carbonate chemistry are simulated according to the OCMIP-2 protocols (Najjar et al., 1999; J. Orr et al., 1999; J. C. Orr et al., 2017; Wanninkhof, 2014; J. Orr & Epitalon, 2015), and gas transfer velocities are scaled with wind speed (Krakauer et al., 2006). The simulated fluxes reproduce large-scale patterns of spatial and seasonal variability (Joos et al., 2025; Müller et al., 2008). The physical ocean component transports tracers through the ocean by advection, convection, and diffusion. Euphotic zone production depends on temperature, light, sea ice cover, and nutrient (phosphate, iron, silica) availability, with a full description of the model biogeochemistry in Parekh et al. (2008), Tschumi et al. (2011) and of carbon isotope dynamics in Jeltsch-Thömmes et al. (2019). In our setup, a fraction of the particulate organic matter formed in the surface ocean is instantly remineralized following an oxygen concentration dependent version of the globally-uniform Martin curve (Battaglia & Joos, 2018) and particulate inorganic carbon and opal dissolution occurs according to globally-uniform e-folding profiles. The remaining solid particles reaching the sediment-ocean interface enter reactive sediments, where they are preserved, remineralized or redissolved depending on dynamically calculated porewater chemistry, and mixed by bioturbation (Jeltsch-Thömmes et al., 2019; Tschumi et al., 2011). The sediment model includes 10 layers and computes fluxes of carbon, nutrients, alkalinity, and isotopes between the ocean, reactive sediments, and the lithosphere.

The ocean is coupled to a 2D atmosphere with dynamic energy and moisture balances and prescribed wind fields and a four-box terrestrial biosphere which exchanges carbon isotopes with the atmosphere.

In the second experiment set (Adloff, Jeltsch-Thömmes, et al., 2024a, 2024b), forcings were scaled either to the  $\delta D$  (Jouzel et al., 2007) or  $\delta^{18}O$  (Lisiecki & Raymo, 2005) records of the last eight glacial cycles. The choice of the isotope record for calculating the instantaneous forcing depends on whether we expect the forcing to evolve synchronously with temperature like  $\delta D$  or have a time lag similar to  $\delta^{18}O$ .

The quantitative results of our study vary between scenarios and are likely model-dependent. All our results were produced with one model and one fixed set of model parameters. The specific values will vary with spatial resolution, different sea-air gas exchange schemes (Müller et al., 2008) and parameterisations for biological and sedimentary carbon cycling. However, the fundamental existence or lack of correlations between carbonate system metrics in our simulations result from the complex interplay of the Earth system as we understand it today and can be reproduced by other models (as shown e.g., for AOU and  $DIC_{org}$  and the non-linear relationship between  $DIC$  and  $CO_2$ ). The exact temporal relationship between carbonate system metrics depends on the applied forcing scenario and as of yet there is no scenario for glacial-interglacial carbon cycle change that is fully consistent with all available proxy data.

Like in Adloff, Jeltsch-Thömmes, et al. (2024a, 2024b), we isolate the effect of each Earth system process for our analysis by subtracting the BASE simulation (orbitally-driven cooling i.e. prescribed in all simulations),

$$fBASE = BASE$$

from simulations with additional processes:

$$fFORC = FORC - fBASE$$

Our simulation output contains the actual  $O_2$  concentration,  $O_2$  concentration at saturation ( $O_{2,sat}$ ) and a tracer for  $O_2$  changes due to air-sea flux changes (i.e., an  $O_2$  tracer i.e. blind to biological processes in the ocean,  $O_{2,sol}$ ) for the surface ocean. With these tracers, we can calculate the physical and biological  $O_2$  disequilibria ( $O_{2,disphys}$  and  $O_{2,disbio}$ ) (Cliff et al., 2021; Schmittner & Fillman, 2024) in the surface ocean:

$$O_{2,disbio} = O_{2,sol} - O_2 \quad (A1)$$

$$O_{2,disphys} = O_{2,sat} - O_2 - O_{2,disbio} = O_{2,sat} - O_{2,sol} \quad (A2)$$

In the water column, we can calculate AOU and BOU (“biological”  $O_2$  utilization), which isolates the effect of changed remineralization and  $O_{2,disbio}$ , as well as  $DIC_{org}$  and  $DIC_{alk}$ , the  $DIC$  resulting from remineralization and  $CaCO_3$  dissolution, respectively:

$$AOU = O_{2,sat} - O_2 \quad (A3)$$

$$BOU = O_{2,sol} - O_2 \quad (A4)$$

$$DIC_{org} = PO_{4,reg} \times 117 \quad (A5)$$

$$DIC_{alk} = ALK_{reg} \times 0.5 \quad (A6)$$

In the manuscript, we present simulation results averaged over the global ocean and/or for four exemplary areas of the ocean (Table A2).



**Table A1**  
*Forcing Scenarios*

ID	Description	LGM-PI amplitude	Modulating proxy
BASE	Orbital changes + radiative effect of greenhouse gasses + ice sheet albedo		CO <sub>2</sub> , CH <sub>4</sub> , δ <sup>18</sup> O
SOWI	BASE + Wind stress strength over Southern Ocean (>48 °S)	−40%	δD
KGAS	BASE + gas transfer velocity in Southern Ocean	−40%	δD
AERO	BASE + Radiative forcing from dust particles	−2.5 W/m <sup>2</sup>	δ <sup>18</sup> O
PHYS	BASE + all physical forcings combined		
LAND	BASE + land C storage	−500 PgC	δ <sup>18</sup> O
REMI	BASE + linear glacial remineralization profile in upper 2000m	linear	δD
PIPO	BASE + PIC:POC changes	−0.33	δD
PO4	BASE + marine PO <sub>4</sub> reservoir	+30%	δ <sup>18</sup> O
BGC	BASE + all biogeochemical forcings combined		
ALL	BASE + all forcings combined		
CO2T	BASE + ALK changes to produce atm. CO <sub>2</sub> consistent with (Bereiter et al., 2015)	−90 ppm	CO <sub>2</sub>

*Note.* Simulations are run in two configurations: The standard setup with interactive sediments and a closed-system setup without sediments (except PO4).

**Table A2**  
*Coordinate Limits of the Example Areas for Which We Visualize the Simulation Results*

Location ID	Latitude (°N)	Longitude (°E)
Iberian Margin	40–47	−14 to −5
North Pacific	40–47	−170 to −159
Eastern Equatorial Pacific	0–4	−102 to −93
Southern Ocean	−64 to −59	−21 to −13

## Appendix B: Local ALK Changes Occur in Closed and Open System and Do Not Follow Stoichiometry

Process stoichiometry can be used to predict ALK changes in an isolated, well-mixed water sample, for example, based on Redfield ratios of decomposing organic matter or dissolution of calcium carbonate (CaCO<sub>3</sub>). A change in organic matter remineralization, for example, would not have a strong effect on ALK in an isolated water parcel. Yet, this is not what is simulated in our experiments for a water parcel in the dynamic ocean. Substantial ALK changes occur in response to the deepening of the mean remineralization depth with and without weathering-burial imbalances and on short and long time scales (Figure S3 in Supporting Information S1). Transport (advection, diffusion, convection) and soft and hard tissue pump feedbacks typically quickly re-distribute ALK within the ocean and overprint the initial stoichiometric effects of any perturbation even in a closed atmosphere-ocean system. Weathering-burial imbalances further alter ALK in the ocean. The ALK changes create the prediction errors in DIC when DIC is estimated from CO<sub>3</sub><sup>2−</sup> only (blue vs. black lines) shown in Figures 1, S1, S2 in Supporting Information S1.

Next, we explain in more detail how these processes operate. We illustrate this for a well oxygenated water column outside of large regional current systems, in this case in the central North Pacific, and for an idealized scenario with a sudden shift in the remineralization profile of organic matter from the upper thermocline toward deeper layers, while leaving the fraction remineralized below 2000 m unchanged. In the real ocean, shifts in the remineralization depth-scale can occur in response to changes in the settling velocities of organic particles, for example, due to water column temperature changes or species shifts in the euphotic zone affecting the particle size spectrum of organic matter export (Armstrong et al., 2001, 2009; Dinuer et al., 2022), or in response to altered kinetic remineralization rates, for example, due to temperature changes (Bendtsen et al., 2002; Laufkötter

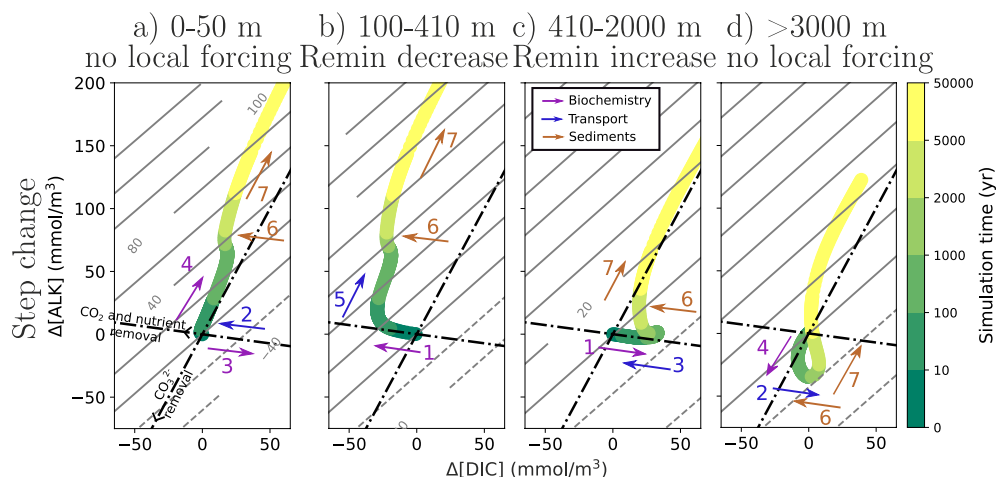
et al., 2017; Taucher et al., 2014). Here, they are prescribed to isolate the biogeochemical effect of the remineralization change from other potential changes in biogeochemical cycles and climate.

Figure B1 shows diagrams of  $\Delta\text{CO}_3^{2-}$  (gray lines) in the  $\Delta\text{DIC}$ - $\Delta\text{ALK}$  space for four depth ranges. In an isolated, well-mixed seawater sample, a change in production or remineralization of organic matter (OM) and  $\text{CaCO}_3$  changes ALK and DIC, and in turn  $\text{CO}_3^{2-}$ , in proportion to the Redfield stoichiometry of organic matter and  $\text{CaCO}_3$ , respectively (black lines in Figure B1). For example, an increase in organic matter remineralization adds DIC to the system and slightly lowers ALK, resulting in a reduction of  $\text{CO}_3^{2-}$ .

This carbonate system theory is incorporated into numerical Earth system models like Bern3D and as such, the immediate local response to a carbonate system perturbation simulated by Bern3D follows the theory.

In our example of shifting remineralization depth of POM, DIC and ALK initially change according to the Redfield ratio of POM, causing a predictable  $\text{CO}_3^{2-}$  decrease in the depth interval (410–2000 m) where net remineralization increases (arrow 1 in Figure B1c) and vice versa where net remineralization decreases (100–410 m; arrow 1 in Figure B1b).

Earth system models like Bern3D also incorporate other dynamic processes, namely large-scale physical transport, air-sea gas exchange and the so-called soft and hard tissue pumps. Advection, diffusion, and convection transport a local perturbation to other water masses. The pumps cycle material between the surface and deep ocean. They involve the production of organic matter and  $\text{CaCO}_3$  from nutrients, DIC, and ALK in the surface and the export of this biogenic matter in particulate and dissolved forms out of the euphotic zone. Organic matter and  $\text{CaCO}_3$  get remineralized at depth, and, closing the cycle, the released nutrients, ALK, and DIC transported by the circulation from the deep back into the euphotic zone.



**Figure B1.** Carbonate system response to a change in remineralization depth. Shown are  $\text{CO}_3^{2-}$  changes (gray contour lines) as a function of ALK and dissolved inorganic carbon changes for different depths in the North Pacific. The contour lines show  $\text{CO}_3^{2-}$  changes, in 20  $\text{mmol/m}^3$  steps, calculated with the MOCSY2.0 carbonate system solver and using respective water mass conditions (temperature, salinity, pressure, phosphate and silicate concentrations) of the pre-industrial model ocean. Solid gray lines show positive values and dotted gray lines show negative values. The response (color) is for a sudden (step-change) shift in remineralization from the upper (100–410 m, panel (b)) to the lower thermocline (410–2000 m, (c), (Figure S20 in Supporting Information S1)) at time zero. Numbered arrows provide a qualitative indication of underlying processes: (1)–primary signal of increased/reduced remineralization due to a change in remineralization rate, (2)–physical transport (e.g., advection) of primary signal, (3)–signal of reduced POC export and remineralization in the water column, (4)–signal of reduced  $\text{CaCO}_3$  export and dissolution in the water column, (5)–physically transported signal of reduced  $\text{CaCO}_3$  export, (6)–whole ocean effect of transiently increased sedimentary POC burial, (7)–whole ocean effect of reduced  $\text{CaCO}_3$  burial (i.e., removal from the ocean). Time is indicated by the color of the respective marker. The black dotted lines show the direction of stoichiometric effects due to the removal/addition of  $\text{CO}_2$  and nutrients by organic matter production/remineralization ( $\text{DIC:ALK} = 117:-17$ ; Paulmier et al., 2009) and removal/addition of  $\text{CO}_3^{2-}$  by  $\text{CaCO}_3$  production/dissolution ( $\text{DIC:ALK} = 1:2$ ) in an isolated water volume.

The soft and hard tissue pumps are linked by the  $\text{CaCO}_3$  production of autotrophic organisms and the circulation and produce spatial gradients in the distribution of nutrients, ALK and DIC. Further, air-sea gas exchange of  $\text{CO}_2$  and, on longer timescales, ocean-sediment interactions and altered weathering impacts tracer distributions. These large-scale processes propagate local biochemical perturbations throughout the water column, resulting in secondary effects in the location of the initial perturbation. In the ocean, a change in remineralization rate has therefore a different net effect on the carbonate system than in an isolated, well-mixed water volume.

New production of organic matter in the euphotic zone is predominantly maintained by relatively fast nutrient recycling from the upper ocean into the euphotic zone. Thus, a scenario where a higher fraction of organic matter export is remineralized deeper and correspondingly a lower fraction in the upper thermocline lowers the rate of nutrient recycling, and thus euphotic zone production (Roth et al., 2014). In our simulation, this effect is almost immediate. Within a few years of the shift in remineralization depth, upwelling of nutrients and local export production is strongly reduced (Figure S13 in Supporting Information S1, effects are shown as arrows 2 and 3 in Figure B1a). The carbonate system effect of reduced POC export in the surface ocean is largely compensated by reduced delivery of POC remineralization products from below. Yet, the coinciding reduction in biogenic  $\text{CaCO}_3$  export leads to an accumulation of DIC and ALK in the surface (arrow 4 in Figure B1a; the slight deviation of the simulated from the Redfield slope may be linked to outgassing of  $\text{CO}_2$  to the atmosphere). After a few years, this  $\text{CaCO}_3$  export signal also propagates to the waters below (arrow 5 in Figure B1b).

Lower export production leads to a reduction of remineralization and  $\text{CaCO}_3$  dissolution below the surface. Thus, at the depths where the remineralization rate was initially increased, the primary carbonate system shift is halted after about 200 years, and reversed over longer timescales due to reduced POC export (arrow 3 Figure B1c).  $\text{CaCO}_3$  mostly falls through the upper water column with little dissolution and predominantly dissolves in the deep ocean. Hence, water masses at intermediate depths with usually high POC remineralization but low  $\text{CaCO}_3$  dissolution, are more strongly affected by the change in POC export. Instead, in the deep ocean, the signal of reduced biogenic  $\text{CaCO}_3$  export dominates, due to a net decrease in  $\text{CaCO}_3$  dissolution (arrow 4 in Figure B1d). Taken together, the secondary effects on the local carbonate system due to changes in vertical transport and export production completely overprint the primary signals of the prescribed remineralization rate shift within decades to centuries in the upper water column (Figures B1a and B1b, dark green colors) and at the latest after one to two millenia at all depths (Figures B1c and B1d, green colors).

The strength of these secondary effects and the timescale for the disappearance of the primary remineralization change signal varies geographically, depending on the magnitude of export production, the abundance of calcifiers, and the intensity of vertical mixing in the upper ocean. In addition, oxygen minimum zones and large-scale circulation patterns influence the vertical distribution of carbonate system changes in response to the prescribed remineralization rate change from the very beginning of the experiment (Figures S10, S11, S12 in Supporting Information S1). For example, in the Eastern Equatorial Pacific (Figure S11 in Supporting Information S1), the presence of oxygen-poor water at intermediate depths shifts the primary net remineralization increase in our simulation to lower depths where aerobic remineralization is possible again. In the North Atlantic (Figure S12 in Supporting Information S1), the strong overturning circulation rapidly transports the surface ocean signals of reduced export production into deeper parts of the water column, overprinting the deep carbonate system shifts that would be expected without advection. Similarly, fast sinking of waters in the Southern Ocean (Figure S10 in Supporting Information S1) transports the primary remineralization signal into the deep ocean, resulting in similar carbonate system shifts throughout the water column between 410 and 5000 m, despite remineralization rates remaining unchanged below 2000 m.

Ocean-sediment interactions further complicate the prediction of local carbonate system changes. These introduce additional feedbacks, namely the burial-nutrient feedback (Roth et al., 2014; Tschumi et al., 2011) and  $\text{CaCO}_3$  compensation (W. S. Broecker & Peng, 1987), on time scales of millenia as well as memory effects (arrows 6–7 in Figure B1, see also Roth et al., 2014, their Figure 3). After about one thousand years, the altered rate and pattern of biogenic particles reaching marine sediments modify the patterns of sedimentary  $\text{CaCO}_3$  dissolution and POC remineralization and the net ocean-sediment fluxes of nutrients, DIC, and ALK. This directly affects the local benthic carbonate system and additionally causes a weathering-burial imbalance on global scale, shifting whole ocean DIC and ALK inventories (arrows 6–7 in Figure B1).

In summary, the evolution of DIC and ALK and, in turn,  $\text{CO}_3^{2-}$ , is the result of a complex interplay of physical and biogeochemical processes in the 3-dimensional atmosphere-ocean-sediment system. While the exact quantitative results shown in Figures 1 and B1 depend on the applied model and the prescribed forcing, we argue that the main findings are robust. Namely, changes in DIC are typically associated with changes in ALK on all timescales. This fact causes generally large prediction errors in DIC when using  $\text{CO}_3^{2-}$  as the sole information (Figure 1).

### Appendix C: The Proportionality of [ALK]-[DIC] and $[\text{CO}_3^{2-}]$ Varies Spatially and Temporally

If ALK changes were known, how well do  $[\text{CO}_3^{2-}]$  changes constrain DIC changes quantitatively? Answering this question requires to examine the spatial and temporal variability of the proportionality constant  $k$  between  $\Delta[\text{ALK}]-\Delta[\text{DIC}]$  and  $\Delta[\text{CO}_3^{2-}]$ . W. Broecker (1982) showed the close correlation of  $\Delta[\text{ALK}]-\Delta[\text{DIC}]$  and  $\Delta[\text{CO}_3^{2-}]$  and Yu et al. (2016) published estimates of  $k$  based on the spatial correlation between these quantities in the Atlantic basin.

In Bern3D, we find the same linear relationship between spatial  $[\text{CO}_3^{2-}]$  and [ALK]-[DIC] in benthic water masses (Figure C1a) as Yu et al. (2016), especially in the Atlantic. The slope of the linearly approximated relationship is less steep in the Pacific and Indian Ocean than in the Atlantic, and we find that it is stable (within uncertainty) over time in simulations with purely physical forcings (as also shown by Yu et al., 2016) but varies over time in simulations with changing the remineralization profile of organic particles, PIC:POC export ratio, terrestrial carbon release and large whole-ocean alkalinity changes (Figure C1b), due to variations in non-carbonate alkalinity and  $[\text{CO}_{2,aq}]$ . Due to this dependence of the relationship between  $[\text{CO}_3^{2-}]$  and [ALK]-[DIC] on local and global biogeochemical changes, the local temporal relationship between  $[\text{CO}_3^{2-}]$  and [ALK]-[DIC] can deviate largely (by more than  $\pm 20\%$ ) from the basin-wide spatial relationship (Figure C2). The applicability of the spatial  $[\text{CO}_3^{2-}]$ -to-[ALK]-[DIC] relationship to temporal carbonate system changes has also been questioned based on box model carbonate system calculations since the pioneering work by Yu et al. (2016), and for example, Farmer et al. (2019) used a  $k = 0.54$  for the Southern Atlantic, derived from experiments with the present-day local carbonate system. Our simulations show that, in addition to spatial heterogeneity in the present-day ocean, variations of the biological pumps and ocean circulation affect the temporal relationship between  $[\text{CO}_3^{2-}]$  and [ALK]-[DIC], in terms of the value of  $k$  and even the linearity of the relationship. The error by assuming a linear temporal relationship is larger for physical forcings and outside the North Atlantic (Figure S13 in Supporting Information S1). Importantly, the possibility of lower  $[\text{CO}_3^{2-}]$  to [ALK]-[DIC] ratios than at present

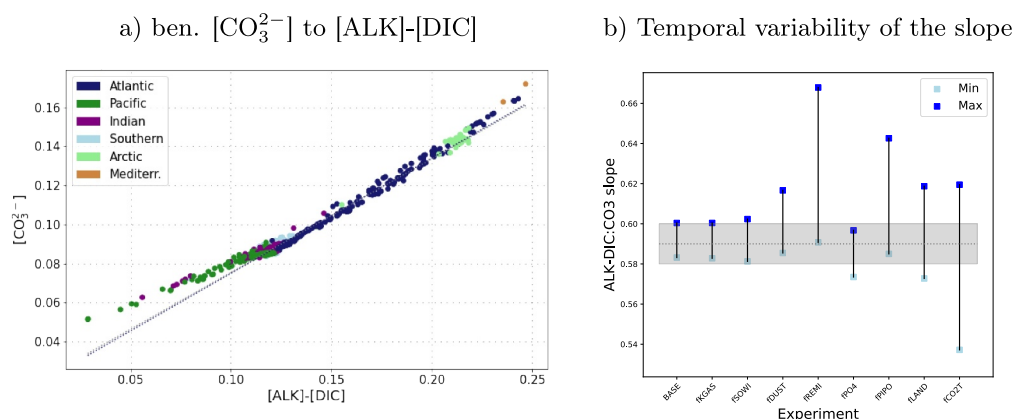


**Figure C1.** (a) Correlation of benthic  $\text{CO}_3^{2-}$  concentrations and the difference of [ALK] and [dissolved inorganic carbon (DIC)], color-coded by ocean basin. The slope of the linearly approximated spatial relationship is 0.59, the same as found by Yu et al. (2016). The data is taken from the pre-industrial state at the end of simulation BASE. (b) Range of the  $[\text{CO}_3^{2-}]$  to [ALK]-[DIC] spatial slope calculated from the benthic Atlantic in each time step of the 780 kyr long simulations. The dotted line with the shaded uncertainty interval shows the slope  $0.59 \pm 0.01$  identified by Yu et al. (2016) in the modern day Atlantic.

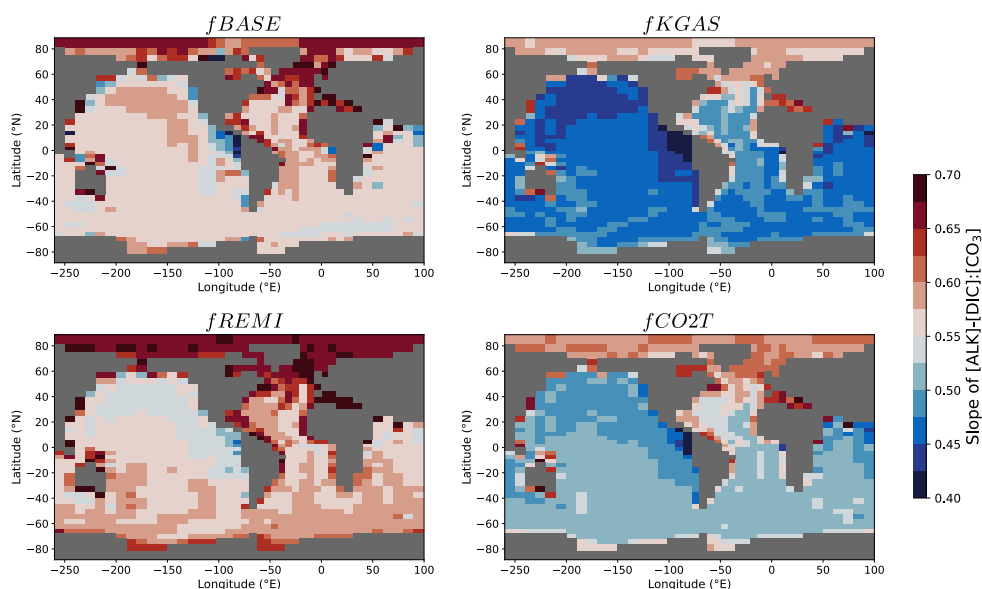


**Figure C2.** Slope of the linearly approximated temporal relationship of  $[\text{CO}_3^{2-}]$  and  $[\text{ALK}]-[\text{DIC}]$  over the last glacial cycle (125 ka–present) for each benthic grid box in various simulations. The slope of the linearly approximated spatial relationship in the benthic Atlantic for the modern ocean is  $0.59 \pm 0.01$ .

means that an assumption of zero alkalinity change does not necessarily provide a minimum estimate for DIC change, as sometimes suggested (Yu et al., 2016, 2020).

The difference in the slope over space versus the slope over time and spatial and temporal variability of these linearly-approximated relationships add to the quantitative uncertainty due to unconstrained alkalinity changes. Simulations with strong perturbations of the biological pump thus show the largest temporal variability of the  $[\text{CO}_3^{2-}]$ -to- $[\text{ALK}]-[\text{DIC}]$  spatial slope, the largest spatial variability in the temporal slope, and alkalinity changes, which increase the quantitative error when applying the modern  $[\text{CO}_3^{2-}]$ -to- $[\text{DIC}]$  spatial relationship to past ocean states and changes.

The sign of past  $[\text{ALK}]$  changes is commonly estimated indirectly, for example, based on  $\text{CaCO}_3$  preservation (Yu et al., 2016, 2020). Our simulations support efforts to combine these with reconstructions of the soft tissue pump (as in e.g., Yu et al., 2019, 2020) and benthic pH to improve the robustness of  $[\text{CO}_3^{2-}]$  interpretations. These additional information add constraints on  $\Delta[\text{ALK}]$  and the accuracy of applying the spatial  $[\text{CO}_3^{2-}]$ -to- $[\text{ALK}]-[\text{DIC}]$  relationship to temporal  $[\text{CO}_3^{2-}]$  changes.

#### Appendix D: The Role of Surface Ocean $\text{O}_2$ Disequilibria in the Predictability of $\text{DIC}_{\text{org}}$ Changes from AOU

The  $\text{O}_2$  concentration in the ocean's interior is determined by the  $\text{O}_2$  concentration of the water at the point of its subduction into the ocean interior and the integrated  $\text{O}_2$  consumption due to aerobic remineralization that occurred since the water left the ocean's surface. The surface ocean  $\text{O}_2$  concentration is in turn determined by the  $\text{O}_2$  solubility and disequilibria between the surface ocean and the air, driven either by physical processes (inhibition of full equilibration e.g., due to obstruction by sea ice or insufficient residence time at the surface) or biological processes ( $\text{O}_2$  deficiency due to aerobic remineralization or  $\text{O}_2$  excess due to primary production).

Figure D1 shows that the local change in the  $\text{DIC}_{\text{org}}$ , that is, the DIC added to a water parcel by organic matter remineralization since it last left the surface ocean, is well tracked by AOU and BOU when we perturb the remineralization profile but cannot be predicted from AOU or BOU when we cool the Earth system.  $\text{DIC}_{\text{org}}$  estimates based on AOU and BOU differ little, suggesting that the main reason for the poor predictive skill is



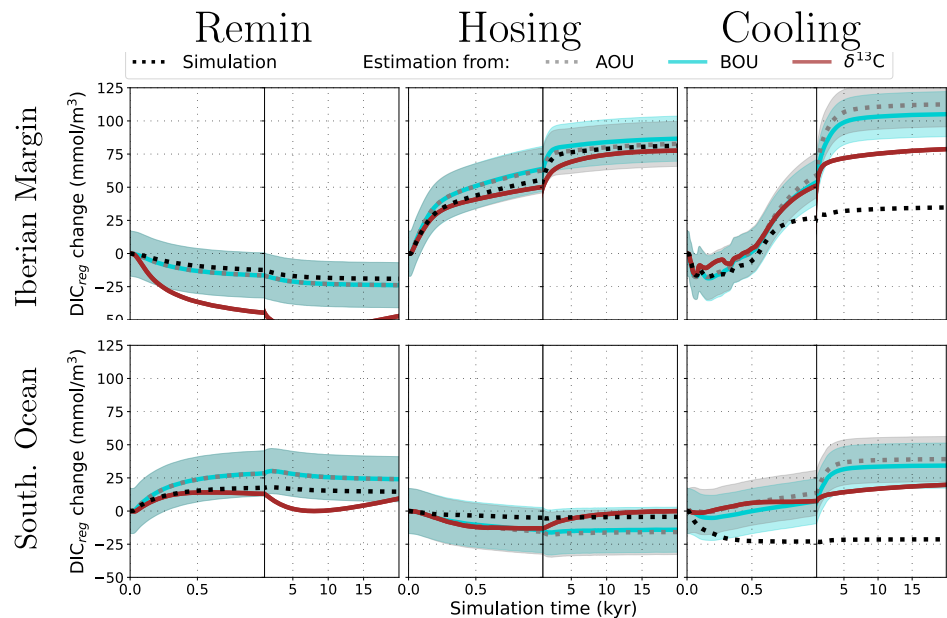


**Figure D1.** Simulated and predicted benthic  $DIC_{org}$  changes due to step changes in various processes over 20 kyr in different oceanographic settings. The simulated  $DIC_{org}$  changes (black line) are compared to the  $DIC_{org}$  changes predicted from simulated apparent oxygen utilization, BOU and  $\delta^{13}C$  changes. The step change in the forced process occurs at time zero. Shown are the simulations with weathering-burial imbalances.

biologically-induced disequilibrium, which is not tracked by either AOU or BOU. This result is consistent across the benthic locations we tested and also valid more generally when averaging over the entire ocean.

Surface ocean disequilibrium changes of  $CO_2$  and  $O_2$ , whether physically or biologically-driven, do not correlate because of the different equilibration times of  $O_2$  and  $CO_2$  between atmosphere and water and the ALK-dependence (and T- and S-dependence) of the DIC portion that is exchangeable between surface ocean and air as  $CO_2$  (Figure D2). This leads to prediction errors.

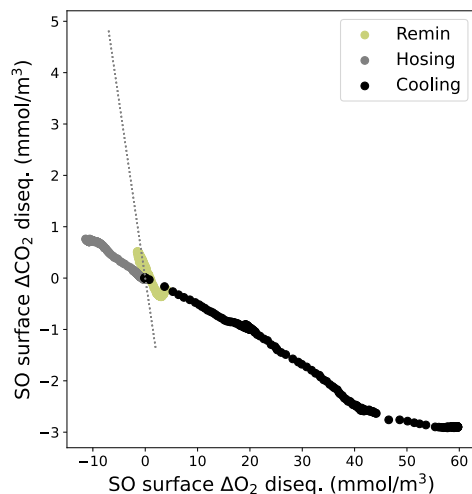


**Figure D2.** Correlation between changes in  $CO_2$  and  $O_2$  disequilibria in the surface of the Southern Ocean ( $>40^\circ S$ ) over 100 kyr in three step change scenarios. The blue dotted line indicates the Redfield ratio of organic export production and remineralization in the model.

Perturbing the remineralization profile (simulation “Remin”) has only a minor effect on the biological  $O_2$  disequilibrium in the surface ocean (Figure D3b). Changes in  $DIC_{org}$  and AOU are then almost exclusively the result of the changing remineralization rate and correlate well in our model with temporally and spatially constant Redfield ratios. A small error is additionally introduced by expansion of anaerobic remineralization, which produces  $DIC_{org}$  without increasing AOU.

If instead of changing the remineralization profile we cool the Earth system (simulation “Cooling”), C and  $O_2$  concentrations in the ocean’s interior are predominantly altered through changes in surface ocean disequilibria, especially biologically-driven disequilibria (similar to the results from Schmittner & Fillman, 2024) and water mass re-distribution. In our simulations, the error made by estimating  $DIC_{org}$  from AOU correlates strongly with the scale of the biologically-driven  $O_2$  disequilibrium in the surface of the Southern Ocean where Southern-sourced waters dominate (Figure D3b).

At the Iberian Margin, water mass re-distributions alter the presence of Southern sourced waters, which adds a second control on the  $DIC_{org}$  error. Generally, increasing the presence of Southern sourced waters at the Iberian Margin increases the  $DIC_{org}$  error (Figure D3c). However, the strength of this control depends on the simultaneous evolution of the  $O_2$  disequilibrium in the surface of the Southern Ocean. In our Hosing scenario, the presence of

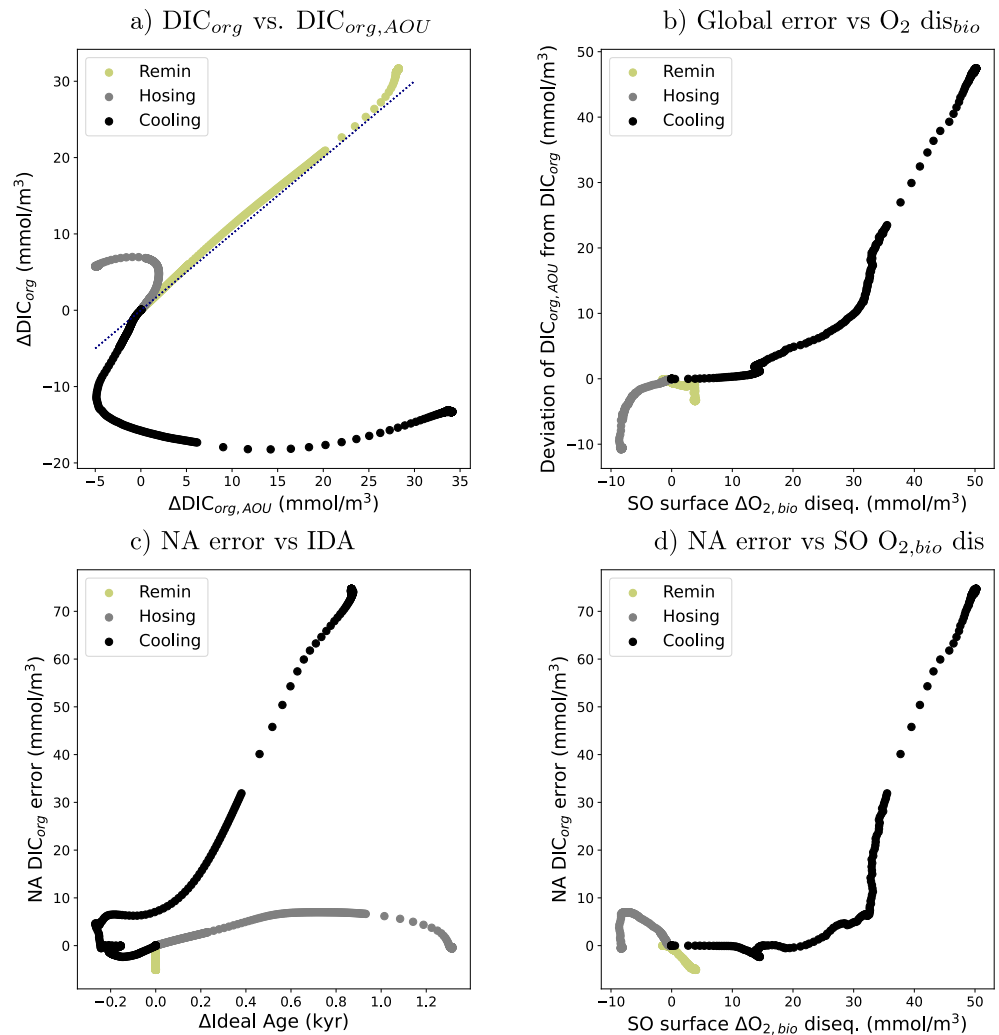


**Figure D3.** (a) Exploration of the mechanisms causing DIC<sub>org</sub> prediction errors over 100 kyr in three step change scenarios (a-b averaged over the whole ocean, c-d at the Iberian Margin). (a) Relationship between simulated DIC<sub>org</sub> changes and those predicted from apparent oxygen utilization changes. The blue dotted line indicates the 1:1 ratio. (b) Relationship between the error of DIC<sub>org,AOU</sub> and changes of the biologically-driven O<sub>2</sub> disequilibrium in the surface of the Southern Ocean. (c-d) Relationship between the error of AOU-derived DIC<sub>org</sub> in benthic water at the Iberian Margin and (c) ideal age in the same water mass and (d) the biologically driven O<sub>2</sub> disequilibrium in the surface Southern Ocean. Increased ideal age at the Iberian Margin signifies an increased presence of Southern sourced water, while reduced ideal age signifies reduced presence of Southern sourced water. Shown are simulations without weathering-burial imbalances.

Southern sourced water at the Iberian Margin is increased (increasing the error) but the O<sub>2</sub> disequilibrium in the surface of the Southern Ocean is simultaneously decreased due to warming (reducing the error, Figure D3d), resulting in an overall relatively small DIC<sub>org</sub> error compared to the Cooling scenario. In our Cooling scenario, AMOC is also weakened in the long-term (after a short-lived initial intensification due to temperature-driven convection, Figure S4 in Supporting Information S1) and thus more Southern sourced water reaches the Iberian Margin. At the same time, the cooling itself increases the O<sub>2</sub> disequilibrium in the surface Southern Ocean and the overall effect on the DIC<sub>org</sub> error is amplified.

Over the simulated glacial cycles, the strong cooling generally leads to large changes in O<sub>2</sub> disequilibria in the surface ocean and thus mismatches between the simulated DIC<sub>org</sub> changes and those predicted from AOU, as shown in Figure D4 for the benthic Southern Ocean. In the “Phys + Bio” scenario in a closed system without sediments the AOU-inferred DIC<sub>org</sub> change closely aligns with the DIC change due to changes in preformed DIC. In this case, preformed DIC is predominantly changed due to productivity and remineralization changes in the

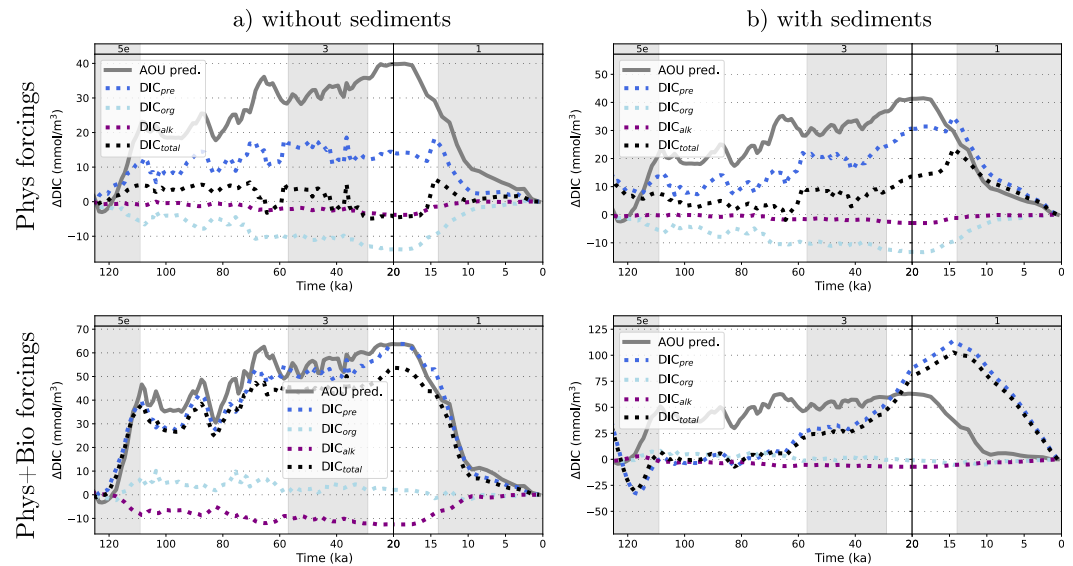


**Figure D4.** Comparison of different components of benthic dissolved inorganic carbon (DIC) changes (dotted lines) to the DIC change predicted from apparent oxygen utilization (gray line) for a simulation of repeated orbitally-paced physical forcing (simulation PHYS from Adloff et al. (2024a, 2024b), top row) and a simulation with additional biogeochemical forcings (simulation ALL from Adloff et al. (2024a, 2024b), bottom row). Results are for our “Southern Ocean” benthic grid cells (Table A2). Gray bars indicate uneven Marine Isotope Stages.

global ocean, which in our model are tied by the Redfield ratio. This is not generally the case but depends on the model set-up and simulation scenario. If, for example, physical processes dominate preformed DIC changes, like in our Phys scenario, or if preformed DIC changes due to weathering-burial imbalances, like in our open system setup, the curves align less well. This confirms that AOU does not generically track the DIC effects of changing surface ocean disequilibrium over glacial cycles Cliff et al. (2021), Schmittner and Fillman (2024) but also shows that there are scenarios in which the error is small.

## Data Availability Statement

We show the results of new simulations and of simulations previously published in Adloff, Jeltsch-Thömmes, et al. (2024a, 2024b). All simulation results are freely available online, including the source code to reproduce the figures in the main manuscript and to further explore the simulation output: Adloff et al. (2025) and Adloff, Jeltsch-Thömmes, et al. (2024a, 2024b).

## References

- Adloff, M., Jeltsch-Thömmes, A., Pöppelmeier, F., Stocker, T. F., & Joos, F. (2024a). Sediment fluxes dominate glacial-interglacial changes in ocean carbon inventory: Results from factorial simulations over the past 780,000 years. *EGU sphere*, 2024, 1–43.
- Adloff, M., Jeltsch-Thömmes, A., Pöppelmeier, F., Stocker, T. F., & Joos, F. (2024b). CP\_Adloff2024\_800kyr (version v0) [Dataset]. Zenodo. <https://doi.org/10.5281/zenodo.11385608>
- Adloff, M., Jeltsch-Thömmes, A., Pöppelmeier, F., Stocker, T. F., & Joos, F. (2025). Simulation output and scripts for Adloff et al. 2025 [Collection]. Zenodo. <https://doi.org/10.5281/zenodo.17112993>
- Anagnostou, E., Huang, K.-F., You, C.-F., Sikes, E., & Sherrell, R. (2012). Evaluation of boron isotope ratio as a pH proxy in the deep sea coral *Desmophyllum dianthus*: Evidence of physiological pH adjustment. *Earth and Planetary Science Letters*, 349, 251–260. <https://doi.org/10.1016/j.epsl.2012.07.006>
- Anderson, R. F., Sachs, J. P., Fleisher, M. Q., Allen, K. A., Yu, J., Koutavas, A., & Jaccard, S. L. (2019). Deep-sea oxygen depletion and ocean carbon sequestration during the last ice age. *Global Biogeochemical Cycles*, 33(3), 301–317. <https://doi.org/10.1029/2018gb006049>
- Armstrong, R. A., Lee, C., Hedges, J. I., Honjo, S., & Wakeham, S. G. (2001). A new, mechanistic model for organic carbon fluxes in the ocean based on the quantitative association of POC with ballast minerals. *Deep Sea Research Part II: Topical Studies in Oceanography*, 49(1–3), 219–236. [https://doi.org/10.1016/s0967-0645\(01\)00101-1](https://doi.org/10.1016/s0967-0645(01)00101-1)
- Armstrong, R. A., Peterson, M. L., Lee, C., & Wakeham, S. G. (2009). Settling velocity spectra and the ballast ratio hypothesis. *Deep Sea Research Part II: Topical Studies in Oceanography*, 56(18), 1470–1478. <https://doi.org/10.1016/j.dsr2.2008.11.032>
- Battaglia, G., & Joos, F. (2018). Marine  $\text{N}_2\text{O}$  emissions from nitrification and denitrification constrained by modern observations and projected in multimillennial global warming simulations. *Global Biogeochemical Cycles*, 32(1), 92–121. <https://doi.org/10.1002/2017gb005671>
- Bendtsen, J., Lundsgaard, C., Middelboe, M., & Archer, D. (2002). Influence of bacterial uptake on deep-ocean dissolved organic carbon. *Global Biogeochemical Cycles*, 16(4), 74–1. <https://doi.org/10.1029/2002gb001947>

## Acknowledgments

This research has been supported by the Schweizerischer Nationalfonds zur Förderung der Wissenschaftlichen Forschung (Grant 200020-200511 and 200020-200492) and Horizon 2020 (Grant 101023443 and 40 820970). Open access publishing facilitated by Universität Bern, as part of the Wiley - Universität Bern agreement via the Consortium Of Swiss Academic Libraries.

- Bereiter, B., Eggleson, S., Schmitt, J., Nehrass-Ahles, C., Stocker, T. F., Fischer, H., et al. (2015). Revision of the EPICA Dome C CO<sub>2</sub> record from 800 to 600 kyr before present. *Geophysical Research Letters*, 42(2), 542–549. <https://doi.org/10.1002/2014gl061957>
- Börker, J., Hartmann, J., Amann, T., Romero-Mujalli, G., Moosdorf, N., & Jenkins, C. (2020). Chemical weathering of loess and its contribution to global alkalinity fluxes to the coastal zone during the Last Glacial Maximum, Mid-Holocene, and Present. *Geochemistry, Geophysics, Geosystems*, 21(7), e2020GC008922. <https://doi.org/10.1029/2020gc008922>
- Boyle, E. A. (1992). Cadmium and  $\delta^{13}\text{C}$  paleochemical ocean distributions during the stage 2 glacial maximum. *Annual Review of Earth and Planetary Sciences*, 20(1), 245–287. <https://doi.org/10.1146/annurev.earth.20.1.245>
- Bradt Miller, L., Anderson, R., Sachs, J., & Fleisher, M. (2010). A deeper respired carbon pool in the glacial equatorial Pacific Ocean. *Earth and Planetary Science Letters*, 299(3–4), 417–425. <https://doi.org/10.1016/j.epsl.2010.09.022>
- Broecker, W. (1982). *Tracers in the sea*. Lamont–Doherty Geological Observatory, Columbia University.
- Broecker, W. S., & Peng, T.-H. (1987). The role of CaCO<sub>3</sub> compensation in the glacial to interglacial atmospheric CO<sub>2</sub> change. *Global Biogeochemical Cycles*, 1(1), 15–29.
- Brovkin, V., Ganopolski, A., Archer, D., & Rahmstorf, S. (2007). Lowering of glacial atmospheric CO<sub>2</sub> in response to changes in oceanic circulation and marine biogeochemistry. *Paleoceanography*, 22(4). <https://doi.org/10.1029/2006pa001380>
- Cartapanis, O., Galbraith, E. D., Bianchi, D., & Jaccard, S. L. (2018). Carbon burial in deep-sea sediment and implications for oceanic inventories of carbon and alkalinity over the last glacial cycle. *Climate of the Past*, 14(11), 1819–1850. <https://doi.org/10.5194/cp-14-1819-2018>
- Cliff, E., Khaliwala, S., & Schmittner, A. (2021). Glacial deep ocean deoxygenation driven by biologically mediated air–sea disequilibrium. *Nature Geoscience*, 14(1), 43–50. <https://doi.org/10.1038/s41561-020-00667-z>
- de Souza, G. F., Vance, D., Sieber, M., Conway, T. M., & Little, S. H. (2022). Re-assessing the influence of particle-hosted sulphide precipitation on the marine cadmium cycle. *Geochimica et Cosmochimica Acta*, 322, 274–296. <https://doi.org/10.1016/j.gca.2022.02.009>
- Dinauer, A., Laufkötter, C., Doney, S. C., & Joos, F. (2022). What controls the large-scale efficiency of carbon transfer through the ocean's mesopelagic zone? Insights from a new, mechanistic model (MSPACMAM). *Global Biogeochemical Cycles*, 36(10), e2021GB007131. <https://doi.org/10.1029/2021gb007131>
- Duplessy, J., Labeyrie, L., Juillet-leclerc, A., Maitre, F., Duprat, J., & Sarnthein, M. (1991). Surface salinity reconstruction of the north-Atlantic ocean during the last glacial maximum. *Oceanologica Acta*, 14(4), 311–324.
- Edwards, N. R., Willmott, A. J., & Killworth, P. D. (1998). On the role of topography and wind stress on the stability of the thermohaline circulation. *Journal of Physical Oceanography*, 28(5), 756–778. [https://doi.org/10.1175/1520-0485\(1998\)028<0756:otrota>2.0.co;2](https://doi.org/10.1175/1520-0485(1998)028<0756:otrota>2.0.co;2)
- Emerson, S., & Archer, D. (1992). Glacial carbonate dissolution cycles and atmospheric pCO<sub>2</sub>: A view from the ocean bottom. *Paleoceanography*, 7(3), 319–331. <https://doi.org/10.1029/92pa00773>
- Farmer, J., Hönsch, B., Haynes, L., Kroon, D., Jung, S., Ford, H., et al. (2019). Deep Atlantic Ocean carbon storage and the rise of 100,000-year glacial cycles. *Nature Geoscience*, 12(5), 355–360. <https://doi.org/10.1038/s41561-019-0334-6>
- Frings, P. J. (2019). Palaeoweathering: How do weathering rates vary with climate? Elements: An International Magazine of Mineralogy. *Geochemistry, and Petrology*, 15(4), 259–265. <https://doi.org/10.2138/gselements.15.4.259>
- Gottschalk, J., Michel, E., Thöle, L. M., Studer, A. S., Hasenfratz, A. P., Schmid, N., et al. (2020). Glacial heterogeneity in southern ocean carbon storage abated by fast South Indian deglacial carbon release. *Nature Communications*, 11(1), 6192. <https://doi.org/10.1038/s41467-020-20034-1>
- Hönsch, B., Ridgwell, A., Schmidt, D. N., Thomas, E., Gibbs, S. J., Sluijs, A., et al. (2012). The geological record of ocean acidification. *Science*, 335(6072), 1058–1063. <https://doi.org/10.1126/science.1208277>
- Humphreys, M. P., Lewis, E. R., Sharp, J. D., & Pierrot, D. (2022). Pyco2sys v1. 8: Marine carbonate system calculations in python. *Geoscientific Model Development*, 15(1), 15–43. <https://doi.org/10.5194/gmd-15-15-2022>
- Ito, T., Follows, M., & Boyle, E. (2004). Is aou a good measure of respiration in the oceans? *Geophysical Research Letters*, 31(17). <https://doi.org/10.1029/2004gl020900>
- Ito, T., & Follows, M. J. (2005). Preformed phosphate, soft tissue pump and atmospheric CO<sub>2</sub>. *Journal of Marine Research*, 63(4), 813–839. <https://doi.org/10.1357/0022240054663231>
- Jaccard, S., Galbraith, E., Sigman, D., Haug, G., Francois, R., Pedersen, T., et al. (2009). Subarctic Pacific evidence for a glacial deepening of the oceanic respired carbon pool. *Earth and Planetary Science Letters*, 277(1–2), 156–165. <https://doi.org/10.1016/j.epsl.2008.10.017>
- Jeltsch-Thömmes, A., Battaglia, G., Cartapanis, O., Jaccard, S. L., & Joos, F. (2019). Low terrestrial carbon storage at the last glacial maximum: Constraints from multi-proxy data. *Climate of the Past*, 15(2), 849–879. <https://doi.org/10.5194/cp-15-849-2019>
- Jeltsch-Thömmes, A., & Joos, F. (2020). Modeling the evolution of pulse-like perturbations in atmospheric carbon and carbon isotopes: The role of weathering–sedimentation imbalances. *Climate of the Past*, 16(2), 423–451. <https://doi.org/10.5194/cp-16-423-2020>
- Jones, I. W., Munhoven, G., Tranter, M., Huybrechts, P., & Sharp, M. J. (2002). Modelled glacial and non-glacial HCO<sub>3</sub><sup>−</sup>, Si and Ge fluxes since the LGM: Little potential for impact on atmospheric CO<sub>2</sub> concentrations and a potential proxy of continental chemical erosion, the marine Ge/Si ratio. *Global and Planetary Change*, 33(1–2), 139–153. [https://doi.org/10.1016/s0921-8181\(02\)00067-x](https://doi.org/10.1016/s0921-8181(02)00067-x)
- Joos, F., Lienert, S., & Zaehle, S. (2025). No increase is detected and modeled for the seasonal cycle amplitude of  $\delta^{13}\text{C}$  of atmospheric carbon dioxide. *Biogeosciences*, 22(1), 19–39. <https://doi.org/10.5194/bg-22-19-2025>
- Jouzel, J., Masson-Delmotte, V., Cattani, O., Dreyfus, G., Falourd, S., Hoffmann, G., et al. (2007). EPICA Dome C ice core 800kyr deuterium data and temperature estimates. IGBP PAGES/World Data Center for Paleoclimatology data contribution series, 91.
- Kerr, J., Rickaby, R., Yu, J., Elderfield, H., & Sadekov, A. Y. (2017). The effect of ocean alkalinity and carbon transfer on deep-sea carbonate ion concentration during the past five glacial cycles. *Earth and Planetary Science Letters*, 471, 42–53. <https://doi.org/10.1016/j.epsl.2017.04.042>
- Khaliwala, S., Schmittner, A., & Muglia, J. (2019). Air–sea disequilibrium enhances ocean carbon storage during glacial periods. *Science Advances*, 5(6), eaaw4981. <https://doi.org/10.1126/sciadv.aaw4981>
- Khesghi, H. S. (2004). Ocean carbon sink duration under stabilization of atmospheric CO<sub>2</sub>: A 1,000-year timescale. *Geophysical Research Letters*, 31(20). <https://doi.org/10.1029/2004gl020612>
- Knox, F., & McElroy, M. B. (1984). Changes in atmospheric CO<sub>2</sub>: Influence of the marine biota at high latitude. *Journal of Geophysical Research: Atmospheres*, 89(D3), 4629–4637. <https://doi.org/10.1029/jd089id03p04629>
- Kobayashi, H., Oka, A., Obase, T., & Abe-Ouchi, A. (2024). Assessing transient changes in the ocean carbon cycle during the last deglaciation through carbon isotope modeling. *Climate of the Past*, 20(3), 769–787. <https://doi.org/10.5194/cp-20-769-2024>
- Krakauer, N. Y., Randerson, J. T., Primeau, F. W., Gruber, N., & Menemenlis, D. (2006). Carbon isotope evidence for the latitudinal distribution and wind speed dependence of the air–sea gas transfer velocity. *Tellus B: Chemical and Physical Meteorology*, 58(5), 390–417. <https://doi.org/10.3402/tellusb.v58i5.17032>
- Kurahashi-Nakamura, T., Paul, A., Merkel, U., & Schulz, M. (2022). Glacial state of the global carbon cycle: Time-slice simulations for the last glacial maximum with an earth-system model. *Climate of the Past*, 18(9), 1997–2019. <https://doi.org/10.5194/cp-18-1997-2022>



- Lacerra, M., Lund, D., Yu, J., & Schmittner, A. (2017). Carbon storage in the mid-depth Atlantic during millennial-scale climate events. *Paleoceanography*, 32(8), 780–795. <https://doi.org/10.1002/2016pa003081>
- Laufkötter, C., John, J. G., Stock, C. A., & Dunne, J. P. (2017). Temperature and oxygen dependence of the remineralization of organic matter. *Global Biogeochemical Cycles*, 31(7), 1038–1050. <https://doi.org/10.1002/2017gb005643>
- Lisiecki, L. E., & Raymo, M. E. (2005). A Pliocene-Pleistocene stack of 57 globally distributed benthic  $\delta^{18}\text{O}$  records. *Paleoceanography*, 20(1). <https://doi.org/10.1029/2004pa001071>
- Lord, N. S., Ridgwell, A., Thorne, M. C., & Lunt, D. J. (2016). An impulse response function for the “long tail” of excess atmospheric  $\text{CO}_2$  in an Earth system model. *Global Biogeochemical Cycles*, 30(1), 2–17. <https://doi.org/10.1002/2014gb005074>
- Moree, A. L., Schwinger, J., Ninnemann, U. S., Jeltsch-Thömmes, A., Bethke, I., & Heinze, C. (2021). Evaluating the biological pump efficiency of the last glacial maximum ocean using  $\delta^{13}\text{C}$ . *Climate of the Past*, 17(2), 753–774. <https://doi.org/10.5194/cp-17-753-2021>
- Müller, S. A., Joos, F., Plattner, G.-K., Edwards, N. R., & Stocker, T. F. (2008). Modeled natural and excess radiocarbon: Sensitivities to the gas exchange formulation and ocean transport strength. *Global Biogeochemical Cycles*, 22(3). <https://doi.org/10.1029/2007gb003065>
- Najjar, R., Orr, J., Sabine, C., & Joos, F. (1999). *Biotic-HowTo*. Internal OCMIP Report, LSCE/CEA Saclay, Gif-sur-Yvette.
- Nowicki, M., DeVries, T., & Siegel, D. A. (2024). The influence of air-sea  $\text{CO}_2$  disequilibrium on carbon sequestration by the ocean's biological pump. *Global Biogeochemical Cycles*, 38(2), e2023GB007880. <https://doi.org/10.1029/2023gb007880>
- Omta, A. W., Follett, C. L., Lauderdale, J. M., & Ferrari, R. (2024). Carbon isotope budget indicates biological disequilibrium dominated ocean carbon storage at the last glacial maximum. *Nature Communications*, 15(1), 8006. <https://doi.org/10.1038/s41467-024-52360-z>
- Orr, J., & Epitalon, J.-M. (2015). Improved routines to model the ocean carbonate system: mocsy 2.0. *Geoscientific Model Development*, 8(3), 485–499. <https://doi.org/10.5194/gmd-8-485-2015>
- Orr, J., Najjar, R., Sabine, C., & Joos, F. (1999). *Abiotic-HowTo*. Internal OCMIP Report, LSCE/CEA Saclay, Gif-sur-Yvette, France, 1999.
- Orr, J. C., Najjar, R. G., Aumont, O., Bopp, L., Bullister, J. L., Danabasoglu, G., et al. (2017). Biogeochemical protocols and diagnostics for the CMIP6 Ocean Model Intercomparison Project (OMIP). *Geoscientific Model Development*, 10(6), 2169–2199. <https://doi.org/10.5194/gmd-10-2169-2017>
- Parekh, P., Joos, F., & Müller, S. A. (2008). A modeling assessment of the interplay between aeolian iron fluxes and iron-binding ligands in controlling carbon dioxide fluctuations during Antarctic warm events. *Paleoceanography*, 23(4). <https://doi.org/10.1029/2007pa001531>
- Paulmier, A., Kriest, I., & Oschlies, A. (2009). Stoichiometries of remineralisation and denitrification in global biogeochemical ocean models. *Biogeosciences*, 6(5), 923–935. <https://doi.org/10.5194/bg-6-923-2009>
- Peterson, C. D., & Lisiecki, L. E. (2018). Deglacial carbon cycle changes observed in a compilation of 127 benthic  $\delta^{13}\text{C}$  time series (20–6 ka). *Climate of the Past*, 14(8), 1229–1252. <https://doi.org/10.5194/cp-14-1229-2018>
- Pöppelmeier, F., Jeltsch-Thömmes, A., Lippold, J., Joos, F., & Stocker, T. F. (2023). Multi-proxy constraints on Atlantic circulation dynamics since the last ice age. *Nature Geoscience*, 16(4), 349–356. <https://doi.org/10.1038/s41561-023-01140-3>
- Qin, B., Li, T., Xiong, Z., Algeo, T. J., & Chang, F. (2017). Deepwater carbonate ion concentrations in the western tropical Pacific since 250 ka: Evidence for oceanic carbon storage and global climate influence. *Paleoceanography*, 32(4), 351–370. <https://doi.org/10.1002/2016pa003039>
- Rae, J. W., Burke, A., Robinson, L., Adkins, J. F., Chen, T., Cole, C., et al. (2018).  $\text{CO}_2$  storage and release in the deep southern ocean on millennial to centennial timescales. *Nature*, 562(7728), 569–573. <https://doi.org/10.1038/s41586-018-0614-0>
- Rae, J. W., Foster, G. L., Schmidt, D. N., & Elliott, T. (2011). Boron isotopes and b/ca in benthic foraminifera: Proxies for the deep ocean carbonate system. *Earth and Planetary Science Letters*, 302(3–4), 403–413. <https://doi.org/10.1016/j.epsl.2010.12.034>
- Rae, J. W. B. (2018). Boron isotopes in foraminifera: Systematics, biomineralisation, and  $\text{CO}_2$  reconstruction. In H. Marschall & G. Foster (Eds.), *Boron isotopes: The fifth element* (pp. 107–143). Springer International Publishing. [https://doi.org/10.1007/978-3-319-64666-4\\_5](https://doi.org/10.1007/978-3-319-64666-4_5)
- Rafter, P. A., Gray, W. R., Hines, S. K., Burke, A., Costa, K. M., Gottschalk, J., et al. (2022). Global reorganization of deep-sea circulation and carbon storage after the last ice age. *Science Advances*, 8(46), eabq5434. <https://doi.org/10.1126/sciadv.abq5434>
- Rickaby, R. E., Elderfield, H., Roberts, N., Hillenbrand, C.-D., & Mackensen, A. (2010). Evidence for elevated alkalinity in the glacial southern ocean. *Paleoceanography*, 25(1). <https://doi.org/10.1029/2009pa001762>
- Roth, R., Ritz, S., & Joos, F. (2014). Burial-nutrient feedbacks amplify the sensitivity of atmospheric carbon dioxide to changes in organic matter remineralisation. *Earth System Dynamics*, 5(2), 321–343. <https://doi.org/10.5194/esd-5-321-2014>
- Sarmiento, J. L., & Toggweiler, J. R. (1984). A new model for the role of the oceans in determining atmospheric  $\text{pCO}_2$ . *Nature*, 308(5960), 621–624. <https://doi.org/10.1038/308621a0>
- Sarnthein, M., Schneider, B., & Groote, P. M. (2013). Peak glacial 14 c ventilation ages suggest major draw-down of carbon into the abyssal ocean. *Climate of the Past*, 9(6), 2595–2614. <https://doi.org/10.5194/cp-9-2595-2013>
- Schmittner, A., Bostock, H. C., Cartapanis, O., Curry, W. B., Filipsson, H. L., Galbraith, E. D., et al. (2017). Calibration of the carbon isotope composition ( $\delta^{13}\text{C}$ ) of benthic foraminifera. *Paleoceanography*, 32(6), 512–530. <https://doi.org/10.1002/2016pa003072>
- Schmittner, A., & Fillman, N. J. (2024). Carbon and carbon-13 in the preindustrial and glacial ocean. *PLOS Climate*, 3(7), e0000434. <https://doi.org/10.1371/journal.pclm.0000434>
- Shao, J., Stott, L. D., Gray, W. R., Greenop, R., Pecher, I., Neil, H. L., et al. (2019). Atmosphere-ocean  $\text{CO}_2$  exchange across the last deglaciation from the boron isotope proxy. *Paleoceanography and Paleoclimatology*, 34(10), 1650–1670. <https://doi.org/10.1029/2018pa003498>
- Siegenthaler, U., & Wenk, T. (1984). Rapid atmospheric  $\text{CO}_2$  variations and ocean circulation. *Nature*, 308(5960), 624–626. <https://doi.org/10.1038/308624a0>
- Sigman, D. M., & Hain, M. P. (2024). Ocean oxygen, preformed nutrients, and the cause of the lower carbon dioxide concentration in the atmosphere of the last glacial maximum. *Paleoceanography and Paleoclimatology*, 39(1), e2023PA004775. <https://doi.org/10.1029/2023pa004775>
- Skinner, L., Primeau, F., Freeman, E., de la Fuente, M., Goodwin, P., Gottschalk, J., et al. (2017). Radiocarbon constraints on the glacial ocean circulation and its impact on atmospheric  $\text{CO}_2$ . *Nature Communications*, 8(1), 16010. <https://doi.org/10.1038/ncomms16010>
- Taucher, J., Bach, L. T., Riebesell, U., & Oschlies, A. (2014). The viscosity effect on marine particle flux: A climate relevant feedback mechanism. *Global Biogeochemical Cycles*, 28(4), 415–422. <https://doi.org/10.1002/2013gb004728>
- Tschumi, T., Joos, F., Gehlen, M., & Heinze, C. (2011). Deep ocean ventilation, carbon isotopes, marine sedimentation and the deglacial  $\text{CO}_2$  rise. *Climate of the Past*, 7(3), 771–800. <https://doi.org/10.5194/cp-7-771-2011>
- Vollmer, T., Ito, T., & Lynch-Stieglitz, J. (2022). Proxy-based preformed phosphate estimates point to increased biological pump efficiency as primary cause of last glacial maximum  $\text{CO}_2$  drawdown. *Paleoceanography and Paleoclimatology*, 37(11), e2021PA004339. <https://doi.org/10.1029/2021pa004339>
- Von Blanckenburg, F., Bouchez, J., Ibarra, D. E., & Maher, K. (2015). Stable runoff and weathering fluxes into the oceans over Quaternary climate cycles. *Nature Geoscience*, 8(7), 538–542. <https://doi.org/10.1038/ngeo2452>



- Wanninkhof, R. (2014). Relationship between wind speed and gas exchange over the ocean revisited. *Limnology and Oceanography: Methods*, 12(6), 351–362. <https://doi.org/10.4319/lom.2014.12.351>
- Yu, J., Anderson, R., Jin, Z., Ji, X., Thornalley, D., Wu, L., et al. (2023). Millennial atmospheric CO<sub>2</sub> changes linked to ocean ventilation modes over past 150,000 years. *Nature Geoscience*, 16(12), 1166–1173. <https://doi.org/10.1038/s41561-023-01297-x>
- Yu, J., Anderson, R. F., Jin, Z., Rae, J. W., Opdyke, B. N., & Eggins, S. M. (2013). Responses of the deep ocean carbonate system to carbon reorganization during the last glacial–interglacial cycle. *Quaternary Science Reviews*, 76, 39–52. <https://doi.org/10.1016/j.quascirev.2013.06.020>
- Yu, J., & Elderfield, H. (2007). Benthic foraminiferal B/Ca ratios reflect deep water carbonate saturation state. *Earth and Planetary Science Letters*, 258(1–2), 73–86. <https://doi.org/10.1016/j.epsl.2007.03.025>
- Yu, J., Elderfield, H., & Piotrowski, A. M. (2008). Seawater carbonate ion- $\delta^{13}\text{C}$  systematics and application to glacial–interglacial north atlantic ocean circulation. *Earth and Planetary Science Letters*, 271(1–4), 209–220. <https://doi.org/10.1016/j.epsl.2008.04.010>
- Yu, J., Foster, G. L., Elderfield, H., Broecker, W. S., & Clark, E. (2010). An evaluation of benthic foraminiferal b/ca and  $\delta^{11}\text{b}$  for deep ocean carbonate ion and ph reconstructions. *Earth and Planetary Science Letters*, 293(1–2), 114–120. <https://doi.org/10.1016/j.epsl.2010.02.029>
- Yu, J., Menviel, L., Jin, Z., Thornalley, D., Barker, S., Marino, G., et al. (2016). Sequestration of carbon in the deep Atlantic during the last glaciation. *Nature Geoscience*, 9(4), 319–324. <https://doi.org/10.1038/ngeo2657>
- Yu, J., Menviel, L., Jin, Z., Thornalley, D., Foster, G. L., Rohling, E., et al. (2019). More efficient North Atlantic carbon pump during the last glacial maximum. *Nature Communications*, 10(1), 2170. <https://doi.org/10.1038/s41467-019-10028-z>
- Yu, J., Oppo, D. W., Jin, Z., Lacerra, M., Ji, X., Umling, N. E., et al. (2022). Millennial and centennial CO<sub>2</sub> release from the Southern Ocean during the last deglaciation. *Nature Geoscience*, 15(4), 293–299. <https://doi.org/10.1038/s41561-022-00910-9>
- Yu, J., Menviel, L., Jin, Z., Anderson, R., Jian, Z., Piotrowski, A., et al. (2020). Last glacial atmospheric CO<sub>2</sub> decline due to widespread Pacific deep-water expansion. *Nature Geoscience*, 13(9), 628–633. <https://doi.org/10.1038/s41561-020-0610-5>
- Zhang, H., Luo, Y., Yu, J., Zhang, L., Xiang, R., Yu, Z., & Huang, H. (2022). Indian Ocean sedimentary calcium carbonate distribution and its implications for the glacial deep ocean circulation. *Quaternary Science Reviews*, 284, 107490. <https://doi.org/10.1016/j.quascirev.2022.107490>